NF

NASA TECHNICAL MEMORANDUM

NASA TM-82474

(NASA-TM-82474) SUNSPOT VARIATION AND SELECTED ASSOCIATED PHENOMENA: A LOOK AT SOLAR CYCLE 21 AND BEYOND (NASA) 38 p
HC A03/MF A01 CSCL 03B G3/92

N82-25069
Unclas
09960

SUNSPOT VARIATION AND SELECTED ASSOCIATED PHENOMENA: A LOOK AT SOLAR CYCLE 21 AND BEYOND

By Robert M. Wilson
Space Sciences Laboratory

February 1982

NASA

George C. Marshall Space Flight Center
Marshall Space Flight Center, Alabama

MSFC - Form 3190 (Rev June 1971)

TECHNICAL REPORT STANDARD TITLE PAGE

1. REPORT NO.	2. GOVERNMENT ACCESSION NO.	3. RECIPIENT'S CATALOG NO.
NASA TM-82474		

4. TITLE AND SUBTITLE	5. REPORT DATE
Sunspot Variation and Selected Associated Phenomena: A Look at Solar Cycle 21 and Beyond	February 1982
	6. PERFORMING ORGANIZATION CODE
7. AUTHOR(S)	8. PERFORMING ORGANIZATION REPORT #
Robert M. Wilson	
9. PERFORMING ORGANIZATION NAME AND ADDRESS	10. WORK UNIT, NO.
George C. Marshall Space Flight Center Marshall Space Flight Center, Alabama 35812	11. CONTRACT OR GRANT NO.
	13. TYPE OF REPORT & PERIOD COVERED
12. SPONSORING AGENCY NAME AND ADDRESS	Technical Memorandum
National Aeronautics and Space Administration Washington, D.C. 20546	14. SPONSORING AGENCY CODE

15. SUPPLEMENTARY NOTES

Prepared by Space Sciences Laboratory, Science and Engineering Directorate.

16. ABSTRACT

This report gives a brief review of solar sunspot cycles 8 through 21. Mean-time intervals are calculated for maximum-to-maximum, minimum-to-minimum, minimum-to-maximum, and maximum-to-minimum phases for cycles 8 through 20 and 8 through 21. Simple cosine functions with a period of 132 years are compared to, and found to be representative of, the variation of smoothed sunspot numbers at solar maximum ($\bar{R}_{MAX}$) and minimum ($\bar{R}_{MIN}$). A comparison of cycles 20 and 21 is given, leading to a projection for activity levels during the Spacelab 2 era (tentatively, November 1984). A prediction is made for cycle 22 (i.e., occurrence dates of $\bar{R}_{MIN}$ and $\bar{R}_{MAX}$ and their corresponding values). Major flares (importance class $\geq$1) are observed to peak several months subsequent to $\bar{R}_{MAX}$ during cycle 21 and to be at minimum level several months after $\bar{R}_{MIN}$. Additional remarks are given for flares, gradual-rise-and-fall (GRF) radio events and 2800-MHz radio emission. The major thrust of this report is to estimate certain solar activity parameters, especially as they relate to the near-term Spacelab 2 timeframe. This report should not be construed to represent a detailed, highly accurate, predictive scheme.

17. KEY WORDS	18. DISTRIBUTION STATEMENT
	Unclassified – Unlimited

19. SECURITY CLASSIF. (of this report)	20. SECURITY CLASSIF. (of this page)	21. NO. OF PAGES	22. PRICE
Unclassified	Unclassified	37	NTIS

TABLE OF CONTENTS

LIST OF ILLUSTRATIONS

LIST OF TABLES

TECHNICAL MEMORANDUM

SUNSPOT VARIATION AND SELECTED ASSOCIATED PHENOMENA: A LOOK AT SOLAR CYCLE 21 AND BEYOND

I. INTRODUCTION

Sunspots are observed to be regions of enhanced magnetic field and to be somewhat cooler and, hence, darker than the surrounding photosphere. They were "discovered" telescopically about 1611; however, naked eye records of large sunspots are now known to have been recorded much earlier [1,2]. Although sunspots are sometimes observed to occur singly, more often they are seen in groups of two or more.

Sunspot cyclic variability (that is, the cyclic change in the number of spots on the Sun with time) was first suggested by Heinrich Schwabe in 1843. Subsequent analysis of observations, both preceding and succeeding this milestone, has confirmed sunspot variability and revealed that the Sun's activity level varies in an approximately cyclic fashion. (Notable exceptions, e.g., the Maunder and Spörer Minima, have been discussed by Eddy [2].)

Daily counts of sunspots are now routinely made at many astronomical observatories around the world. These daily sunspot numbers[1] are averaged, thereby yielding mean monthly sunspot numbers (e.g., the Zürich sunspot number, denoted R_z) which are further averaged, in a particular way, to yield a smoothed sunspot number or 13-month running mean, as it is sometimes called.[2] The variation of the smoothed sunspot number with time is inherently less noisy than the "raw" mean

---

1. Sunspot number R is defined as

$$R = k\,(10\,g + f) \quad , \tag{1}$$

where f is the total number of spots observed regardless of size, g is the number of observed spot groups, and k is a normalization parameter which varies from observatory to observatory to bring counts into agreement by accounting for telescope size, atmospheric opacity, etc.

2. Smoothed sunspot number $\bar{R}_{13}$ is defined [3] as

$$\bar{R}_{13} = \frac{R_{+6} + R_{-6} + 2\sum_{i=-5}^{+5} R_i}{24} \quad , \tag{2}$$

where R_{+6} is the mean monthly sunspot number 6 months ahead of the month of interest, R_{-6} the mean monthly number 6 months behind the month of interest, and $\sum_{i=-5}^{+5} R_i$ is the sum of the mean monthly sunspot numbers 5 months either side and including the month of interest.

sunspot number, while still appropriately showing the general trend and level of solar activity; thus, it is much more suitable for the statistical comparisons and predictions of this report. Month-to month mean sunspot numbers vary, by as little as a few percent to as much as 30 percent or more, with variation usually being greatest at solar minimum.

Sunspot variation or the sunspot cycle (or activity cycle), as it is more commonly known [4], has been reliably determined, based on daily sunspot counts, back to about 1848, corresponding to the maximum of solar cycle number 9. (The solar cycle has been traced back further in time, but the data are much less reliable.) Therefore, solar physicists and prognosticators tend to examine contemporary cycles (present cycle is number 21) and predict future cycles in the light of all cycles since cycle 8, the milestone cycle.

The purpose of this report is fourfold. First, it will briefly review sunspot cycles 8 through 20 in terms of time variation and $\bar{R}_{13}$ values at maxima and minima. Second, it will give results pertaining to the decline of cycle 20 and the minimum, ascending, and maximum phases of cycle 21, based on sunspot number, 2800-MHz radio flux, frequency of flare occurrence (major flares and, separately, all flares), and frequency of occurrence of gradual-rise-and-fall (GRF) radio events, which may be associated with eruptive prominences and coronal transients (e.g., Sheeley et al. [5], Webb et al. [6], Smith et al. [7], and Fisher et al. [8]). The associations between these latter parameters and $\bar{R}_{13}$ are discussed. Third, a prediction is made for expected levels of activity for the Spacelab 2 era (late 1984), and, lastly, a prediction is made for cycle 22. The analysis of cycles 20 through 21 is based on data obtained from the NOAA Solar Geophysical Data (Prompt Reports), Boulder, Colorado (abbreviated SGD in this report).

II. SUNSPOT CYCLES 8 THROUGH 20

Allen [9] has tabulated the dates of occurrence for solar cycle maximum and minimum and values of smoothed sunspot number at cycle maximum ($\bar{R}_{MAX}$) and minimum ($\bar{R}_{MIN}$) for all solar cycles since 1700. Utilizing these data, simplified solar activity cycles (beginning with cycle 8) were drawn and are illustrated in Figure 1. Basically, Figure 1 represents the envelopes of $\bar{R}_{MAX}$ and $\bar{R}_{MIN}$ (the dark lines at the top and bottom of the figure, respectively). The numbered triangles represent each of the solar cycles (8 through 21).

Means for $\bar{R}_{MAX}$ and $\bar{R}_{MIN}$ have been calculated, based on the Allen tabulated parameters, for cycles 8 through 20 and 8 through 21. They are $\bar{R}_{MAX}$ = 116.2 and 121.9 and $\bar{R}_{MIN}$ = 5.2 and 5.7, respectively. Maxima range between 64.2 and 201.3 and minima between 1.5 and 12.4.

Figure 2 depicts the duration interval (in years) versus solar cycle number for solar cycles 8 through 21; the intervals measured are sunspot maximum to subsequent maximum (MAX-MAX), minimum to subsequent minimum (MIN-MIN), maximum to subsequent minimum (MAX-MIN), and minimum to subsequent maximum (MIN-MAX). (Please note that this report follows the standard convention of beginning a cycle at minimum

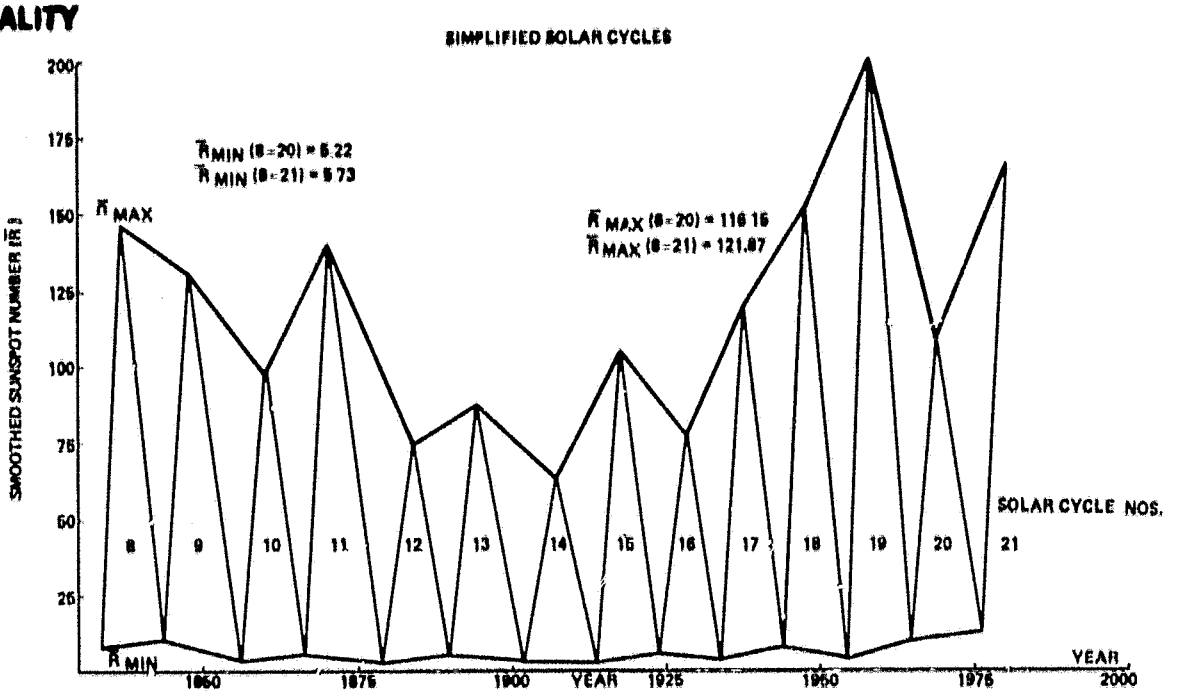

Figure 1. Solar activity cycles, simplified to two data points ($\bar{R}_{MAX}$ and $\bar{R}_{MIN}$) per cycle, this plot shows envelopes over the maxima and minima of 13 numbered cycles (cycles 8 through 21).

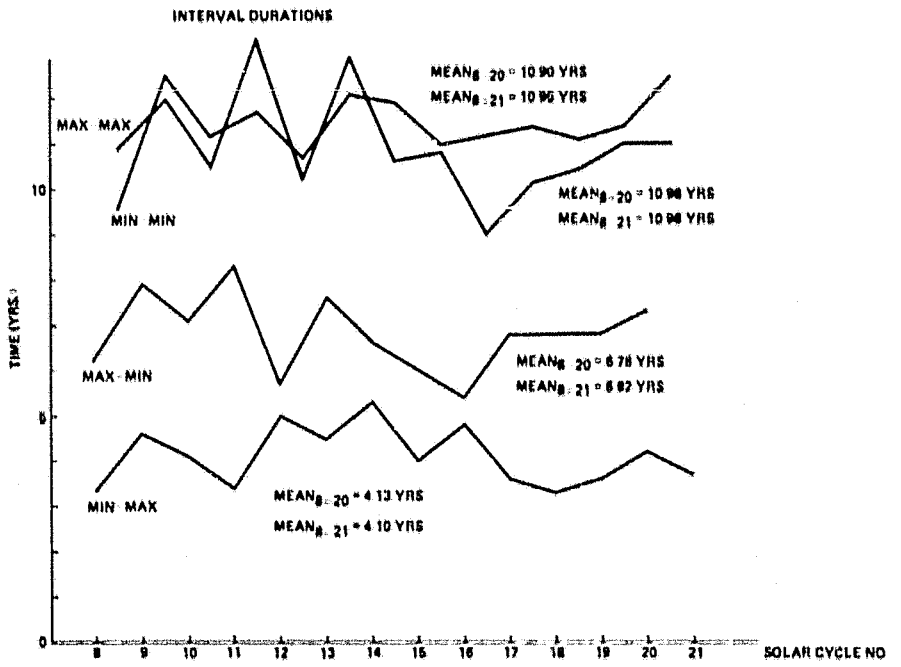

Figure 2. Cycle interval curves. Time intervals in years are plotted for each solar cycle for maximum to subsequent maximum (MAX-MAX), minimum to subsequent minimum (MIN-MIN), maximum to subsequent minimum (MAX-MIN), and minimum to subsequent maximum (MIN-MAX). Thus, MAX-MAX and MAX-MIN curves are for intercycle values, whereas MAX-MIN and MIN-MAX are for intracycle values. Mean values for each interval are given in years for cycles 8 through 20 and 8 through 21.

occurrence and ending it at subsequent cycle minimum occurrence. Also, note that, in Figure 2, MAX-MAX and MIN-MIN are arbitrarily plotted at the mid-points between cycle numbers and MAX-MIN and MIN-MAX are plotted on the cycle number.) Means for these parameters are given in Table 1. MAX-MAX values range from 9.0 to 13.3 years (mean ∿ 11 years), MIN-MIN from 9.6 to 12.5 years (mean ∿ 11 years), MAX-MIN from 5.4 to 8.3 years (mean ∿ 6.8 years), and MIN-MAX from 3.3 to 5.3 years (mean ∿ 4.1 years).

TABLE 1. MEAN TIME INTERVAL SOLAR CYCLE PARAMETERS

	Mean Time Intervals: Months (Years)	
	Cycles 8-20	Cycles 8-21
MAX-MAX	131.8 (10.98)	131.8 (10.98)
MIN-MIN	130.8 (10.90)	131.4 (10.95)
MAX-MIN	81.4 (6.78)	81.8 (6.82)
MIN-MAX	49.6 (4.13)	49.2 (4.10)

Examination of Figure 1 suggests that, perhaps, $\bar{R}_{MAX}$ and $\bar{R}_{MIN}$ are related, in some way, to a periodic function, since values for $\bar{R}_{MAX}$ and $\bar{R}_{MIN}$ appear to peak around cycles 8 and 9 and 19 through 21 and are of minimum value around cycles 14 and 15. In Figure 3, the data of Figure 1 are recast into a plot of $\bar{R}_{MAX}$ and $\bar{R}_{MIN}$

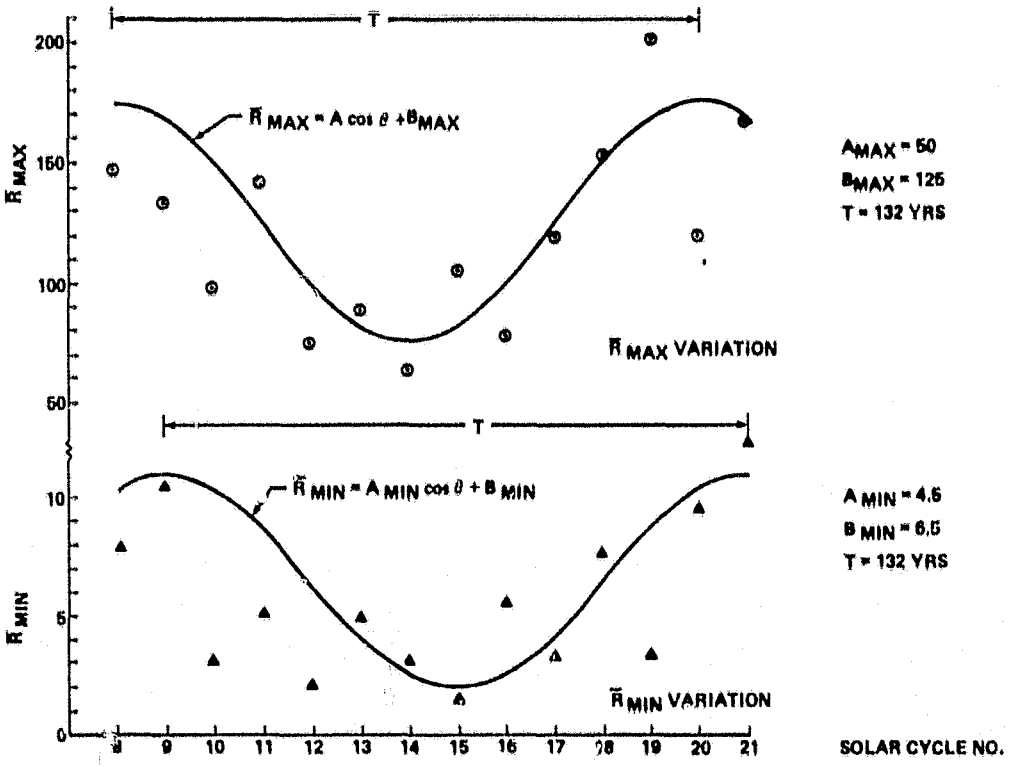

Figure 3. Cosine-fit to $\bar{R}_{MAX}$ and $\bar{R}_{MIN}$ values versus cycle number.

against solar cycle number. The curves drawn through these data points are arbitrarily selected, simple cosine functions having a period of 132 years (which coincidentally is ≈ 1.5 times the Gleissberg cycle [1]). Although the functions were chosen arbitrarily and do not represent a best fit, a fairly good fit, commensurate with about 30 percent error bars or less, is obtained (for $\bar{R}_{MAX}$). (Clearly, a straight-line fit is not suggested.) One observes that for $\bar{R}_{MAX}$ and $\bar{R}_{MIN}$ cycle 21 follows that of cycle 9, cycle 22 that of cycle 10, and so on. In this way the solar cycle variation takes on a truly periodic appearance postdicting values for $\bar{R}_{MAX}$ and $\bar{R}_{MIN}$ that, for the most part, have been close to actual values.

III. SUNSPOT CYCLES 20 THROUGH 21

In this section, a prediction for cycle 21 dates of occurrence and $\bar{R}$ values for sunspot cycle minimum and maximum, based on Table 1 means and Figure 3 curves in conjunction with observed occurrence dates of minimum and maximum of sunspot cycle 20, is compared to actual dates of occurrence and $\bar{R}$ values for sunspot cycle 21 minimum and maximum. Also discussed is the association between 2800 MHz emission level and sunspot number and the variation of number of major flares, number of flares (in general), and number of GRF events with time (in particular, phase of solar cycle). The relationship between these latter parameters and sunspot number is examined and a determination made as to whether the ascending portion of a cycle is significantly different from its descending portion. These relationships will be helpful for determining flare activity levels during the Spacelab 2 era (Section IV).

Sunspot cycle 20 began with a minimum in September 1964 having a value of $\bar{R}_{MIN}$ equal to 9.6; maximum occurred in October 1968 with a value of $\bar{R}_{MAX}$ equal to 110.6. Thus, based on the MIN-MIN time interval for cycles 8 through 20, September 1975 would be projected to be the minimum for cycle 21; and based on the MAX-MAX time interval for cycles 8 through 20, the maximum for cycle 21 would occur approximately October 1979. The actual dates of sunspot minimum and maximum were March 1976 and December 1979. Thus, using mean time intervals the occurrences of sunspot minimum could be predicted to within 6 months and maximum to within 2 months.

Based on Figure 3, $\bar{R}_{MIN}$ for cycle 21 would have been predicted to be about 11 and $\bar{R}_{MAX}$ to be about 168. Actual values for $\bar{R}_{MIN}$ and $\bar{R}_{MAX}$ for cycle 21 were 12.4 and 166.3, respectively (i.e., to within about one-unit discrepancy for $\bar{R}_{MIN}$ and to within about two-units discrepancy for $\bar{R}_{MAX}$).

Figure 4 plots the mean monthly Zürich sunspot number (R_z), the smoothed sunspot number ($\bar{R}_{13}$), the mean monthly 2800-MHz radio flux corrected to one astronomical unit (F_{2800}), and the smoothed 2800-MHz radio flux ($\bar{F}_{13}$), calculated similarly to $\bar{R}_{13}$ [equation (2)] for the time period February 1969 through December 1980, or the period covering the descending portion of cycle 20 and the minimum, ascending and maximum portions of cycle 21. Observe that the time interval from the maximum of cycle 20 to the maximum of cycle 21 was 134 months; the time interval from the maximum of cycle 20 to the minimum of cycle 21 was 89 months; and the time interval

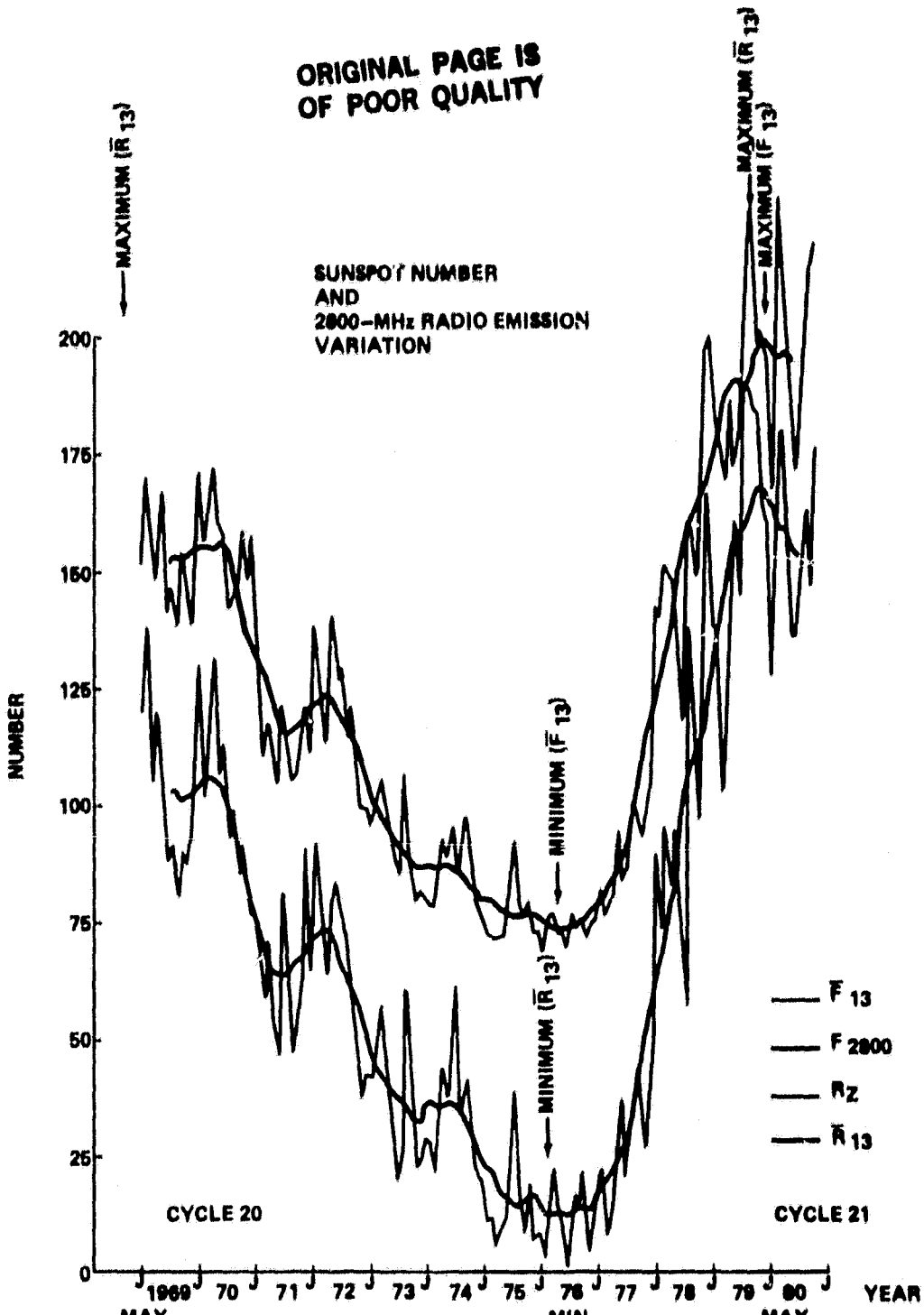

Figure 4. Cycles 20 and 21. R_z, $\bar{R}_{13}$, F_{2800}, and $\bar{F}_{13}$ are plotted in terms of numbers versus month for the period January 1969 through December 1980. The dates of occurrence of maximum $\bar{R}_{13}$ and $\bar{F}_{13}$ and minimum $\bar{R}_{13}$ and $\bar{F}_{13}$ are shown.

for the ascending portion of cycle 21 (minimum to maximum) was 45 months. Also, observe that $\bar{F}_{13}$ and $\bar{R}_{13}$ maxima, minima, and trends are essentially the same and are, thus, very linearly related. $\bar{F}_{13}$ minimum occurs approximately 3 months after $\bar{R}_{13}$ minimum, and $\bar{F}_{13}$ maximum occurs approximately 2 months after $\bar{R}_{13}$ maximum. Scatter associated with $\bar{F}_{13}$ values is approximately 20 percent or less and is, thus, a smoother signal for statistical comparisons than $\bar{R}_{13}$. (Scatter diagrams for R_z versus $\bar{R}_{13}$, F_{2800} versus $\bar{F}_{13}$, and other flare and eruptive parameters versus their smoothed numbers are given in the Appendix.)

Figure 4, in addition to showing variation of $\bar{F}_{13}$ and $\bar{R}_{13}$ with time, depicts the cycles in terms of solar cycle phase (assuming a period of 134 months, based on cycle 20 maximum to cycle 21 maximum). Thus, the descending portion of cycle 20 accounts for 66.4 percent of the period and the ascending portion of cycle 21 for 33.6 percent. If the fall of cycle 20 and the rise of cycle 21 are statistically typical of any solar cycle, then the ratio of ascending to descending periods is about 0.5, or the descending portion of a cycle is on the order of twice as long as its ascending portion.

If solar minimum is thought of as an interval when $\bar{R}_{13}$ was within 2.25 units of $\bar{R}_{13}$ (=13.5), then observe that cycle 21 minimum was about 21 months in length (between May 1975 and January 1977). During this interval the mean $\bar{R}_{13}$ was $14.54\ ^{+2.24}_{-2.10}$. Similarly, if solar maximum is regarded as an interval when $\bar{R}_{13}$ was within six units of $\bar{R}_{MAX}$, then observe that cycle 21 maximum was approximately 13 months in duration (between July 1979 and July 1980), and the mean $\bar{R}_{13}$ was $160.25\ ^{+6.03}_{-4.62}$. The ratio of maximum period to minimum period is about 0.6, or the minimum period is about 1.5 times the length of the maximum period.

The descent phase of cycle 20, based on Figure 4, is marked by the occurrence of three major "bumps" in $\bar{R}_{13}$ (and $\bar{F}_{13}$). The first bump occurred approximately 18 months after $\bar{R}_{MAX}$ cycle 20 and was about 19 percent higher than a smooth fall-off in sunspot number. The second bump occurred 42 months after $\bar{R}_{MAX}$ cycle 20 and was about 44 percent higher. The third bump occurred 67 months after $\bar{R}_{MAX}$ cycle 20 and was 40 percent higher. Thus, the descending portion of cycle 20 had periods of enhanced activity and was not a simple, smoothly decaying function. It is noteworthy that the Skylab missions fortuitously occurred during the third bump, approximately 2 to 3 years prior to solar minimum and that, in addition to increased sunspot number during this period, there was an increase in flare activity as well (as explained in later paragraphs and by Wilson [10]).

Figure 5 plots the ratio of $\bar{F}_{13}$ to $\bar{R}_{13}$ and F_{2800} to R_z. Observe the peak ratio of $\bar{F}_{13}$ to $\bar{R}_{13}$ to be about 6, occurring at $\bar{R}_{13}$ minimum for cycle 21. The lowest ratio was 1.17, occurring approximately 1 month prior to $\bar{R}_{13}$ maximum for cycle 21, and, though not shown, a similar ratio is suggested for $\bar{R}_{MAX}$ cycle 20.

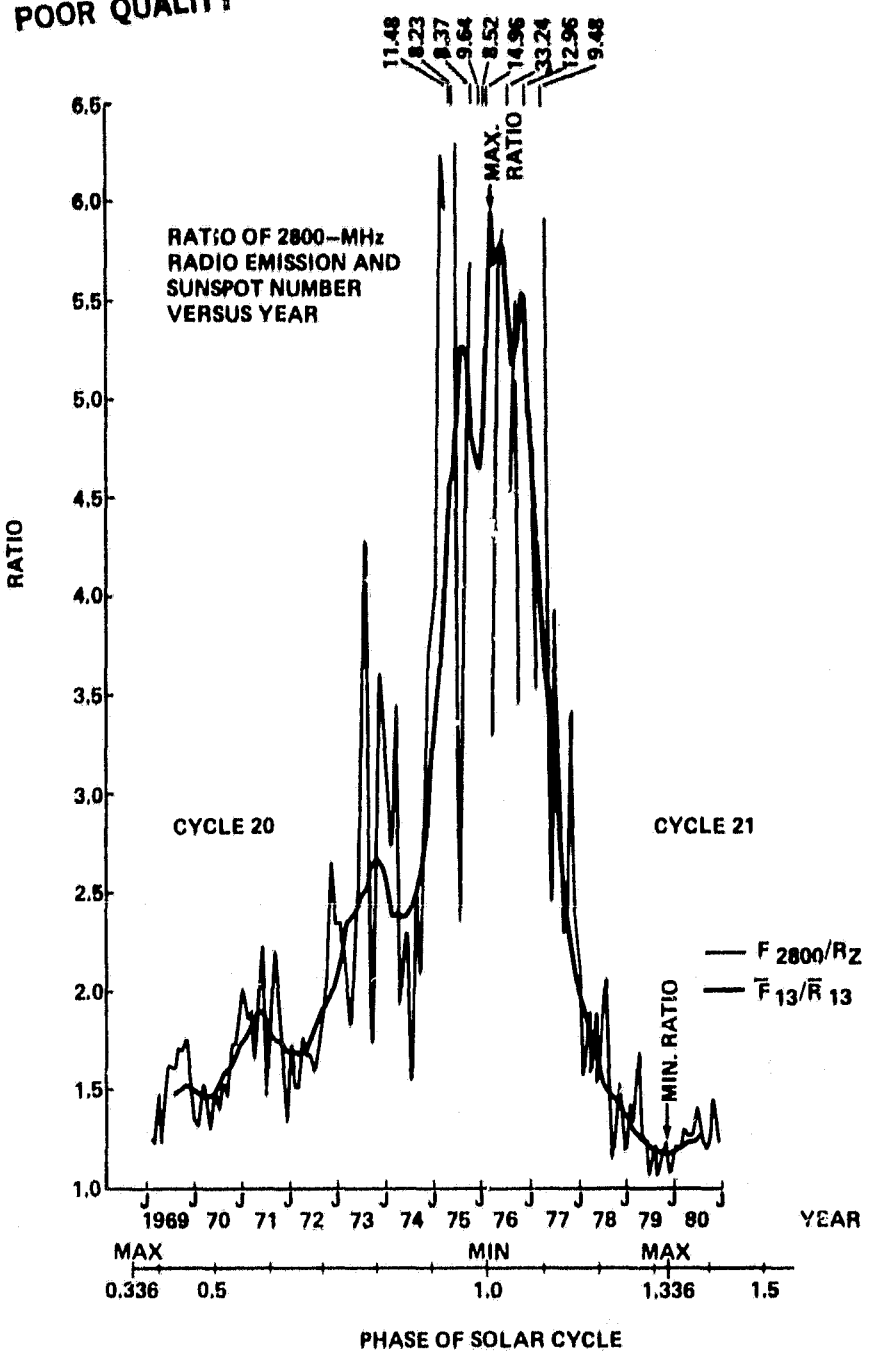

Figure 5. Variation of F_{2800}/R_z and $\bar{F}_{13}/\bar{R}_{13}$ for cycles 20 and 21. The maximum and minimum ratio values are denoted.

Figure 6 depicts the number [N (≥1)] of flares per month and smoothed number [$\bar{N}_{13}$ (≥1)] of flares of optical importance greater than or equal to 1 versus time (for definition of "importance," see [11]). It can be observed that the period of minimum flare occurrence corresponds essentially to the same period of minimum sunspot number, being approximately 21 months in length (approximately May 1975 to January 1977), and to have a mean value of $\bar{N}_{13}$ (≥1) equal to $4.01\ ^{+1.57}_{-1.55}$. (Monthly mean numbers ranged from 0 to 15 during this interval.) The peak period of major flare

activity, with much greater monthly scatter, occurred during 1980; the mean value of N_{13} (≥1) was 63.89 $^{+7.57}_{-5.81}$ for the first 8 months of 1980. Note that the minimum N_{13} (≥1) value occurred approximately 7 months after minimum $\bar{R}_{13}$ value and that the maximum $\bar{N}_{13}$ (≥1) value also appears to follow maximum $\bar{R}_{13}$ value by 7 months. The ascending portion of cycle 21 appears to be somewhat more monotonic than the descending portion of cycle 20, in terms of N_{13} (≥1). Bumps in the N_{13} (≥1) curve during the descending portion of cycle 20, similar and corresponding to bumps in R_{13}, are noted, although they clearly are not as distinctive as those of R_{13}.

Figure 7 displays the number (N) and smoothed number (N_{13}) of all flares, both major flares and subflares, versus time from the minimum period of cycle 21 through the maximum phase. (The plot was limited to times subsequent to late 1975 because of the change in the style of presentation of flare data in the SGD; subsequent to late 1975, flare data were contained in one listing and all observations of a single flare were grouped together, making flare count determination simple.) It is observed that minimum $\bar{N}_{13}$ occurrence coincides with minimum $\bar{N}_{13}$ (≥1) occurrence, approximately 7 months after minimum $\bar{R}_{13}$ occurrence. Maximum $\bar{N}_{13}$ occurrence appears to have peaked 5 months prior to maximum $\bar{R}_{13}$ and 12 months prior to maximum N_{13} (≥1) occurrences, although considerable variability is noted in 1979 and 1980. (Also, the smoothed data are only plotted through August 1980.) Individual N values were greatest in 1980, being nearly 800 in December. Note the very linear appearance of the $\bar{N}_{13}$ curve during the ascending portion of cycle 21, suggesting perhaps a linear relationship with $\bar{R}_{13}$.

Figure 8 shows the ratio of N (≥1) to N and the smoothed ratio of N (≥1) to N for the same time period as Figure 7. The minimum in the smoothed ratio occurred approximately 4 months after minimum $\bar{R}_{13}$ and approximately 3 months prior to minimum $\bar{N}_{13}$ (≥1). The ratio varied linearly with time from early 1976 until about mid-1978, when the mean ratio dipped (for approximately 1 year), and also between mid-1979 and the peak occurrence in mid-1980. The maximum smoothed ratio is observed to coincide with the maximum $\bar{N}_{13}$ (≥1) occurrence, approximately 7 months after maximum $\bar{R}_{13}$ occurrence.

Figure 9 illustrates the number [N(GRF)] and smoothed number [$\bar{N}_{13}$ (GRF)] of radio determined GRF events, based on the SGD. The data plotted cover the descending portion of cycle 20 and the minimum and ascending portions of cycle 21. The bumps in GRF values, during the descending portion of cycle 20, correspond to the bumps previously mentioned in the sunspot number and flare count curves (Figs. 4 and 6); i.e., the large bump in 1972 corresponds to the second bump in the $\bar{R}_{13}$ curve, the second bump in the GRF curve to the third bump in the $\bar{R}_{13}$ curve, and the third bump with the hint of a fourth bump in the $\bar{R}_{13}$ curve, very close to minimum conditions. The minimum N_{13} (GRF) value coincides with minimum $\bar{N}_{13}$ (≥1) occurrence, approximately 7 months

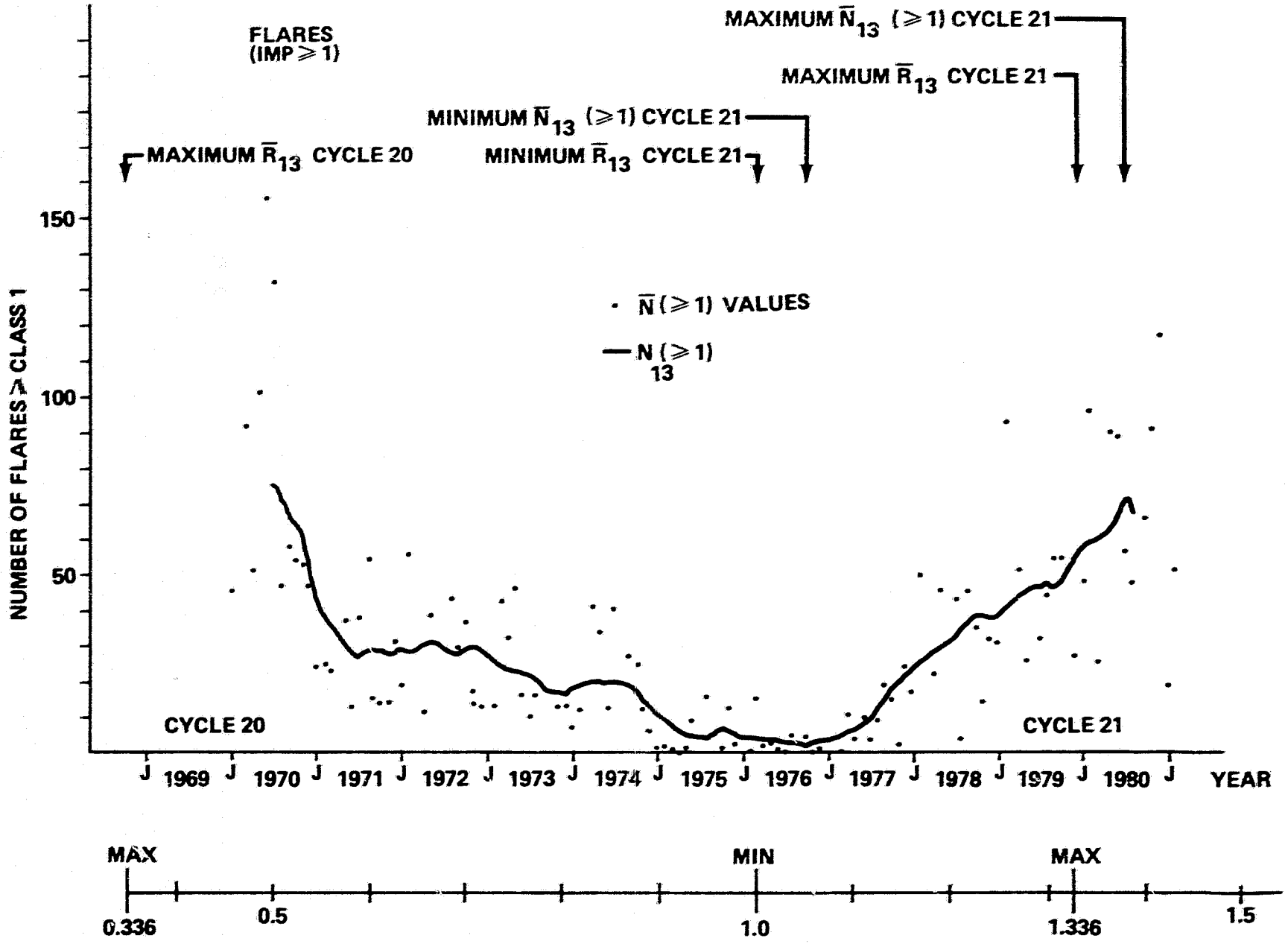

Figure 6. Variation of $\bar{N}_{13}$ (≥1) for cycles 20 and 21.

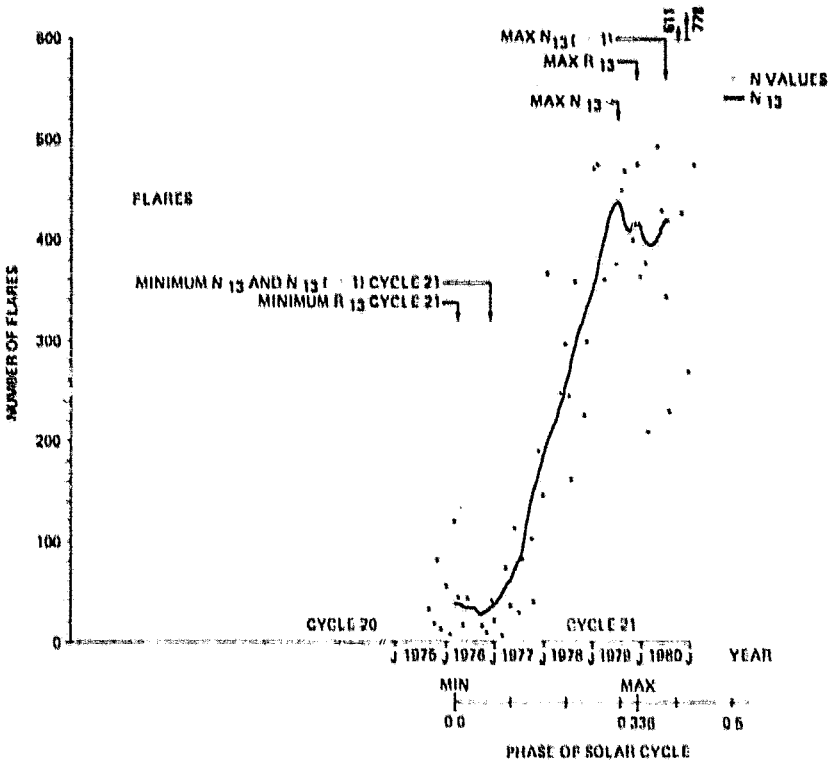

Figure 7. Variation of $\bar{N}_{13}$ for cycle 21.

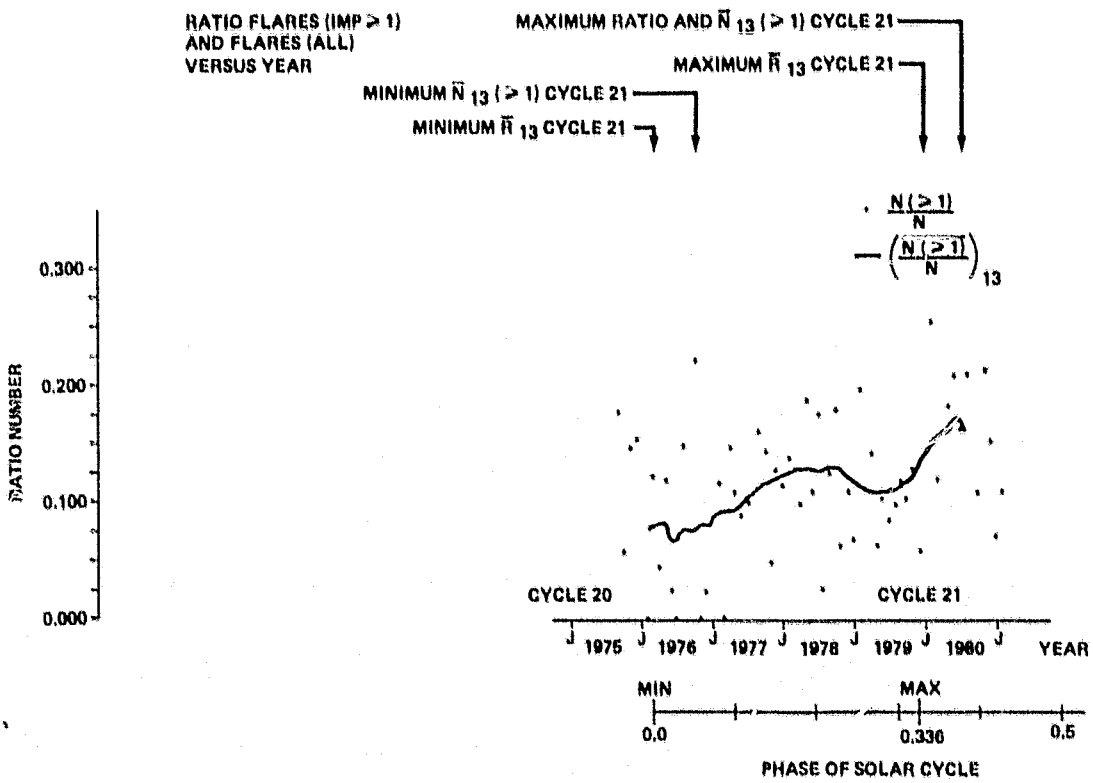

Figure 8. Variation of $\overline{(N\ (\geq 1)/N_{13}}$ for cycle 21.

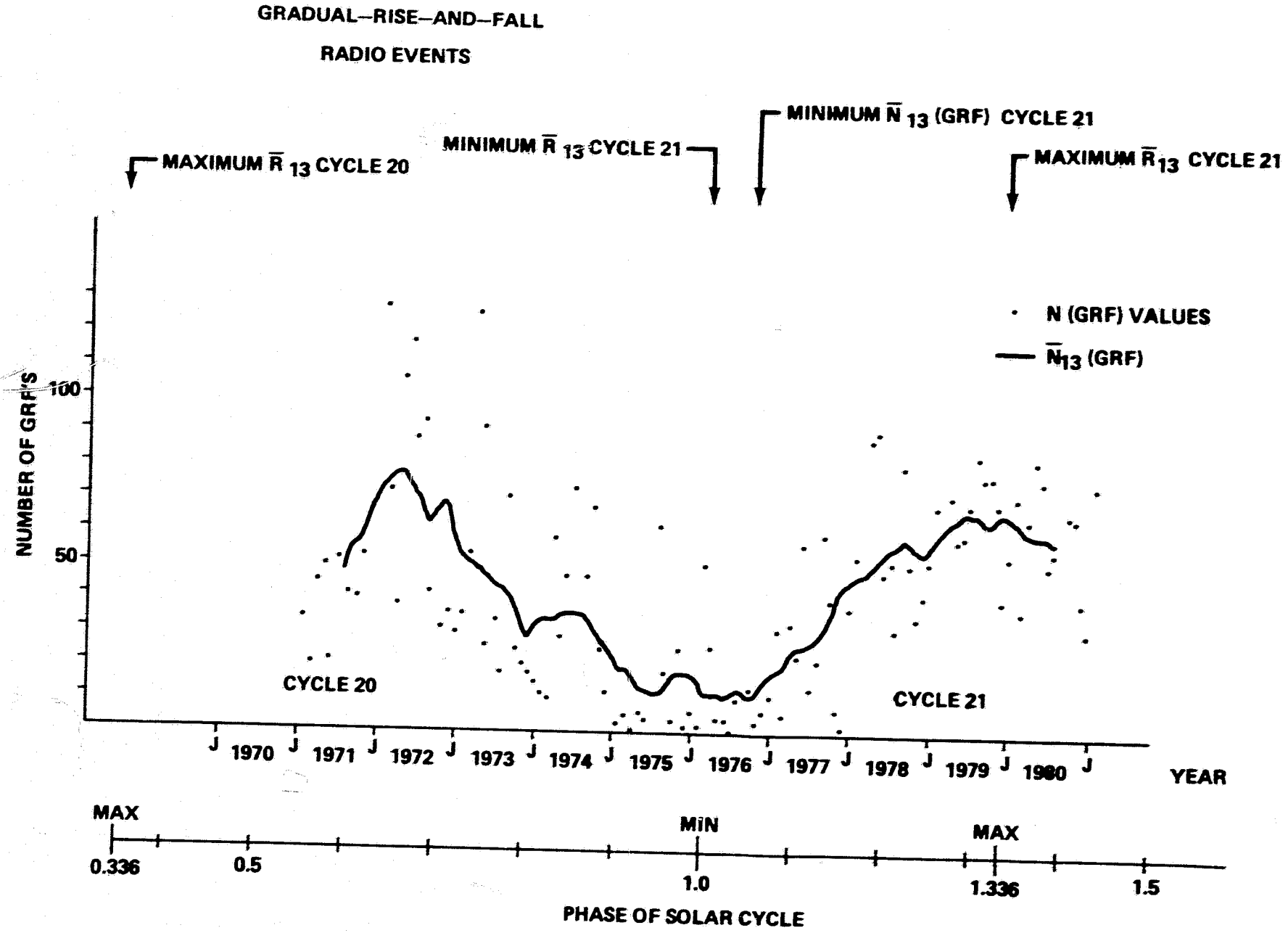

Figure 9. Variation of $\bar{N}_{13}$ (GRF) for cycles 20 and 21.

following minimum $\bar{R}_{13}$ occurrence. The maximum $\bar{N}_{13}$ (GRF) occurrence is about August 1979 or approximately 4 months prior to maximum $\bar{R}_{13}$ occurrence, being nearly coincidental in time with $\bar{N}_{13}$ occurrence.

While sunspot activity was considerably higher in cycle 21 than in cycle 20, it is to be noted that Figures 6 and 9 suggest that flare and eruptive activity may have been somewhat higher in cycle 20 rather than cycle 21. While numbers of flares and eruptives may be linearly related to sunspot number within a cycle or portions of two cycles, they may not be exactly related between successive cycles or any two randomly chosen cycles. Insufficient data are available to define the general relationships (if any).

As hinted previously, the smoothed data during the ascending portion of cycle 21 suggest somewhat linear relationships between flares, eruptives, and 2800 MHz radio emission with sunspot number. Figure 10 depicts the relationship between $\bar{N}_{13}$ (≥1) and $\bar{R}_{13}$. Line A denotes the straight line extending from the origin to the maximum $\bar{R}_{13}$ value; hence, it covers the ascending portion of cycle 21. Line D connects the origin with the maximum $\bar{N}_{13}$ (≥1) value; hence, it may be loosely regarded as the best-guess for the descending portion of cycle 21. Lines C_1 and C_2 correspond to the best-fit component lines for the ascending portion of the data set; i.e., C_1 covers the values $12 \leq \bar{R}_{13} \leq 62$ and C_2 the values $62 \leq \bar{R}_{13} \leq 165$. The line equations are stated below:

Line A (Ascending Cycle 21) $$\bar{N}_{13} (\geq 1) = 0.34\, \bar{R}_{13} \quad , \tag{3}$$

Line D (Descending Cycle 21) $$\bar{N}_{13} (\geq 1) = 0.46\, \bar{R}_{13} \quad , \tag{4}$$

Line C_1 (Cycle 21, $12 \leq \bar{R}_{13} \leq 62$) $$\bar{N}_{13} (\geq 1) = 0.52\, \bar{R}_{13} - 6 \quad , \tag{5}$$

and

Line C_2 (Cycle 21, $62 \leq \bar{R}_{13} \leq 165$) $$\bar{N}_{13} (\geq 1) = 0.23\, \bar{R}_{13} + 11.5 \quad . \tag{6}$$

Figure 10 clearly shows that the maximum $\bar{N}_{13}$ (≥1) did not occur at the maximum $\bar{R}_{13}$ value. It occurred 7 months following sunspot maximum at a value of $\bar{R}_{13}$ within 6 percent of the maximum $\bar{R}_{13}$ value. The maximum $\bar{N}_{13}$ (≥1) value exceeded by about 35 percent the equation-predicted value (Line A), given $\bar{R}_{13}$. Thus, Figure 10 suggests that the descending portion of cycle 21 will be somewhat more active, in a proportionate way, than the ascending portion; or, in other words, major flares appear to be more prevalent just after and into the declining or late phases of the solar cycle, rather than in the rising or early phases of the cycle. Component C_1 spanned 21 months and component C_2 about 23 months; thus $\bar{R}_{13}$ was increasing at the rate of about 2.38 units per month in the initial phases of the rising portion of cycle 21 and at the rate of 4.48 units per month in the latter stages of the ascending portion of the cycle. Similarly, $\bar{N}_{13}$ (≥1) increased at the rate of 0.67 flares per month during C_1 and at the rate of 1.04 flares per month during C_2.

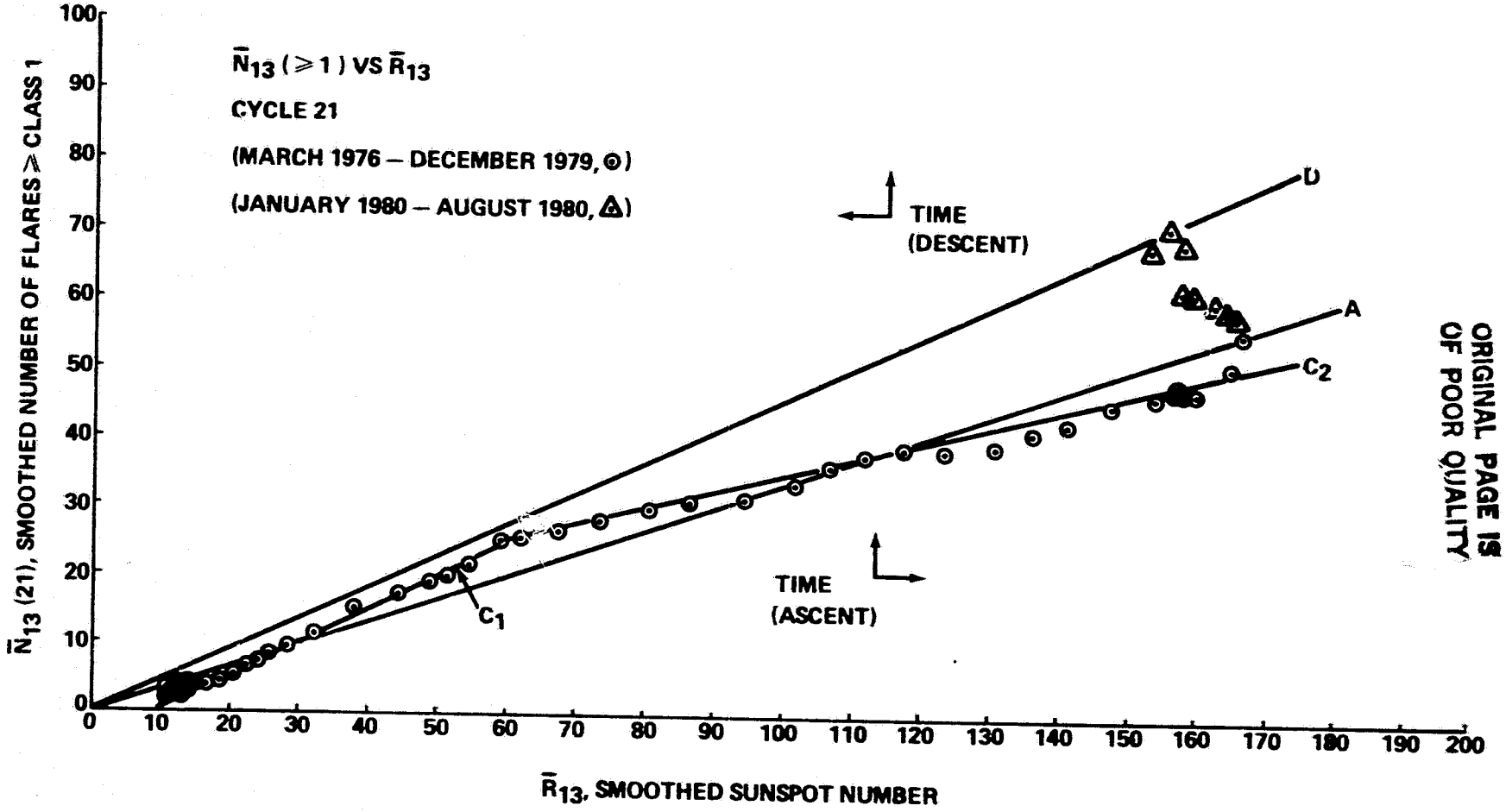

Figure 10. $\bar{N}_{13}$ (≥1) versus $\bar{R}_{13}$ for ascending portion (Θ) and descending portion (△) cycle 21. Line equations given in text.

Figure 11 illustrates the relationship between $\bar{N}_{13}$ and $\bar{R}_{13}$. Line A essentially corresponds to the ascending portion of cycle 21, connecting the initial plot point with the maximum N_{13} value, and line D to the descending portion, connecting the initial plot point to the maximum $\bar{R}_{13}$ N_{13} value. The line equations are:

$$\text{Line A (Ascending Cycle 21)} \qquad \bar{N}_{13} = 2.83\ \bar{R}_{13} - 1.5 \tag{7}$$

and

$$\text{Line D (Descending Cycle 21)} \qquad \bar{N}_{13} = 2.50\ \bar{R}_{13} \tag{8}$$

Figure 11 shows that flare activity (subflares and major flares) peaked prior to the maximum R_{13} value, implying that, since major flare counts peaked subsequent to sunspot number maximum, the number of subflares peaked prior to maximum $\bar{R}_{13}$ occurrence. Hence, the early phases of the solar cycle appear to be marked by the occurrence of many subflares, while the descending portion may be somewhat less prolific in subflare production. At maximum $\bar{R}_{13}$, the value of $\bar{N}_{13}$ was approximately 9 percent below that predicted by equation (7) (Line A). $\bar{R}_{13}$ increased at the rate of 3.58 units per month and $\bar{N}_{13}$ increased at the rate of 10.68 flares per month, based on line A.

Figure 12 depicts the relationship between $\bar{N}_{13}$ (GRF) and $\bar{R}_{13}$. Line A is a parabola which corresponds to the ascending portion of cycle 21, and line D is a straight line approximation pertaining to the descending portion of the cycle. The line equations are given below:

$$\text{Line A (Ascending Cycle 21)} \qquad \bar{N}_{13}\ (\text{GRF}) = \sqrt{20\ (\bar{R}_{13} - 12)} + 12 \tag{9}$$

and

$$\text{Line D (Descending Cycle 21)} \qquad \bar{N}_{13}\ (\text{GRF}) = 0.36\ \bar{R}_{13} + 7.5\ . \tag{10}$$

The behavior of $\bar{N}_{13}$ (GRF) appears to follow that of $\bar{N}_{13}$ in that peak numbers slightly precede maximum $\bar{R}_{13}$ occurrence and that there is an indication that the number of GRF events during the descending portion of cycle 21 will be lower than during the ascending portion.

Figure 13 shows the linear relationship between $\bar{F}_{13}$ and $\bar{R}_{13}$. Although a linear equation (Line A, including dashed-line extension) is commensurate with the data (being less than 7 percent error at large $\bar{R}_{13}$ values), the data indicate a slope change at $\bar{R}_{13}$ values greater than 110. The line equations during the ascending and probably the descending portions of cycle 21 are:

$$\text{Line A (all } \bar{R}_{13}\text{, especially } 13 \leq \bar{R}_{13} \leq 110) \qquad \bar{F}_{13} = 0.89\ \bar{R}_{13} + 63 \tag{11}$$

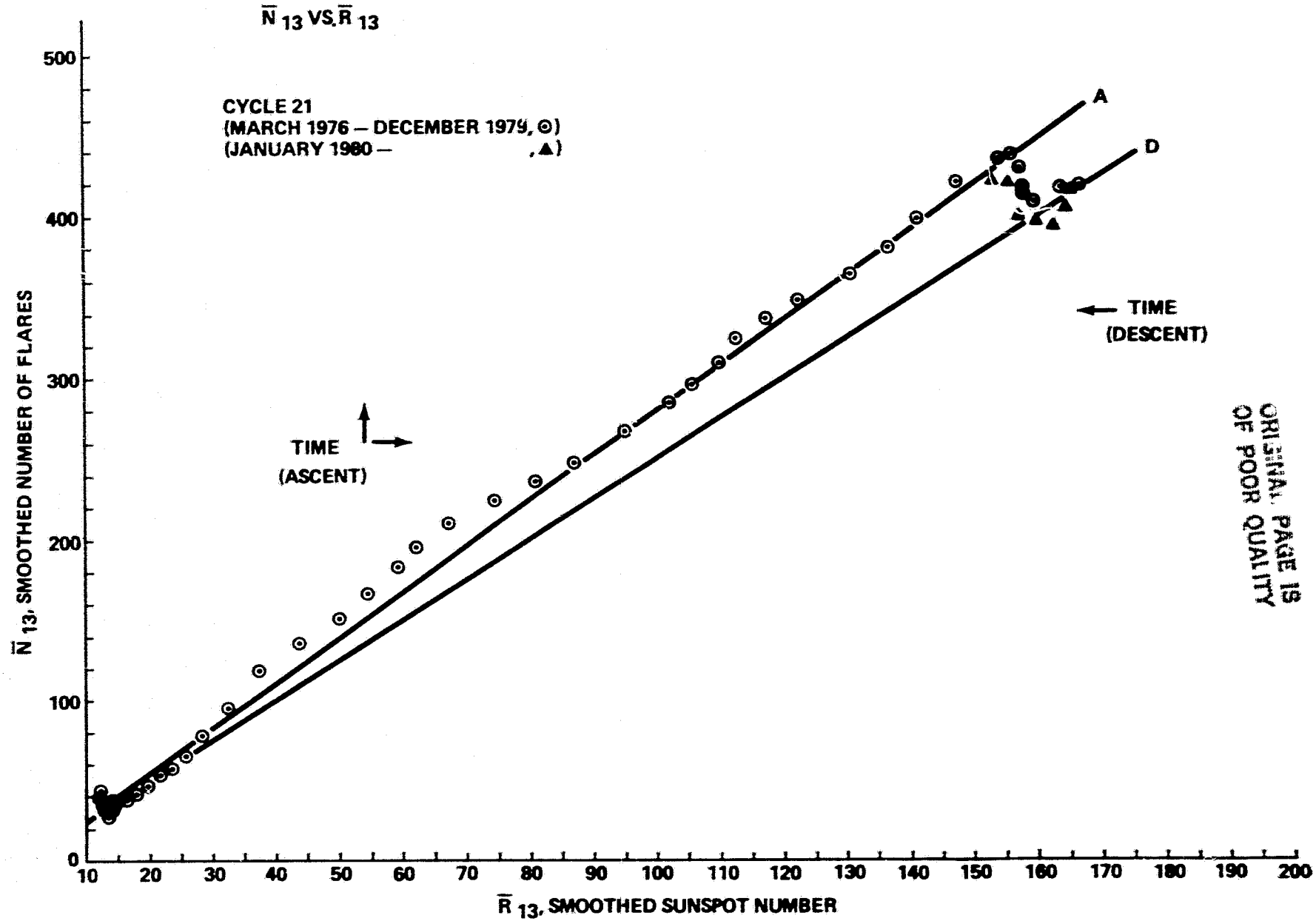

Figure 11. $\bar{N}_{13}$ versus $\bar{R}_{13}$ for ascending portion (⊙) and descending portion (▲) cycle 21. Line equations given in text.

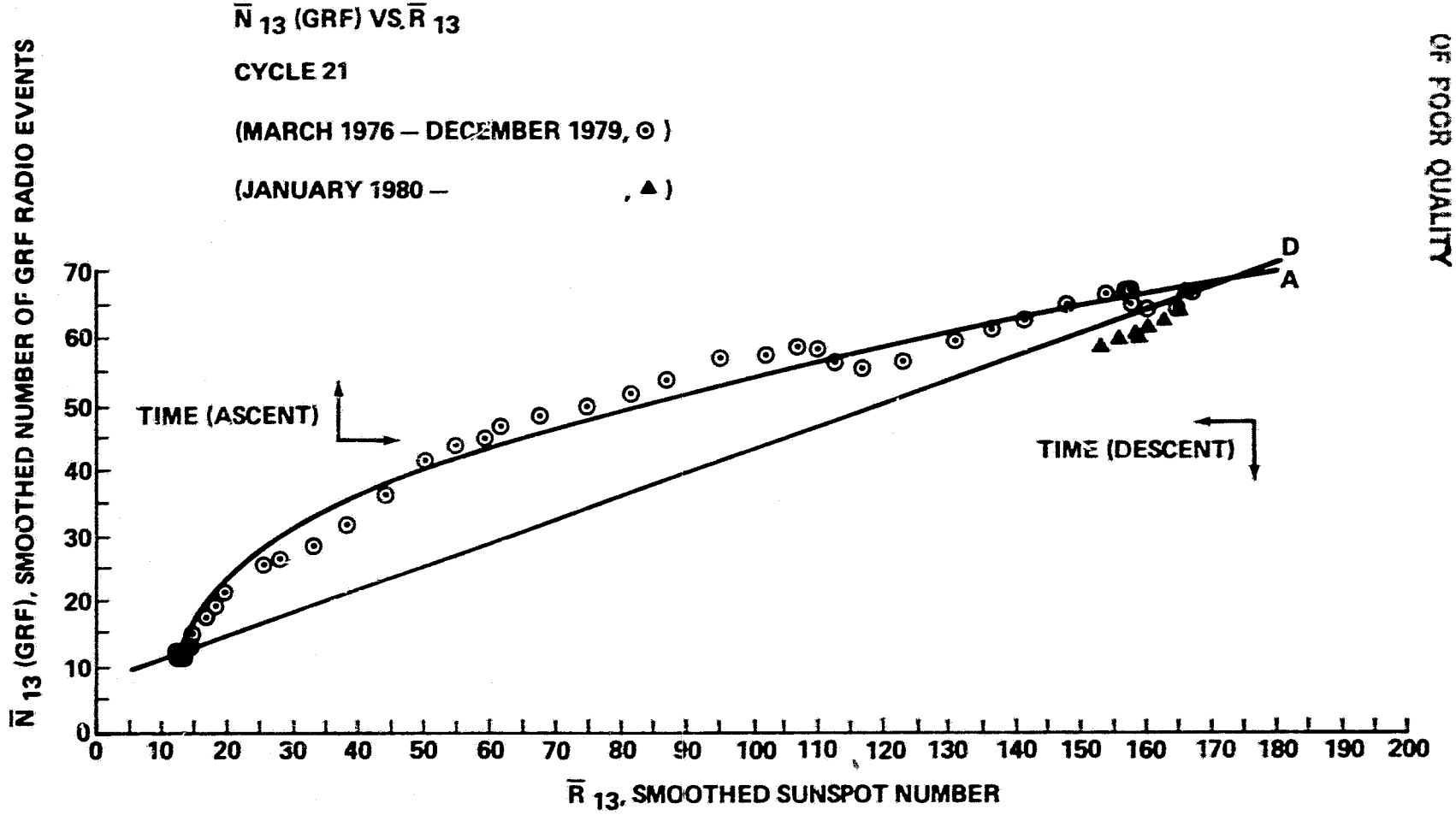

Figure 12. $\bar{N}_{13}$ (GRF) versus $\bar{R}_{13}$ for ascending portion (⊙) and descending portion (▲) cycle 21. Line equations given in text.

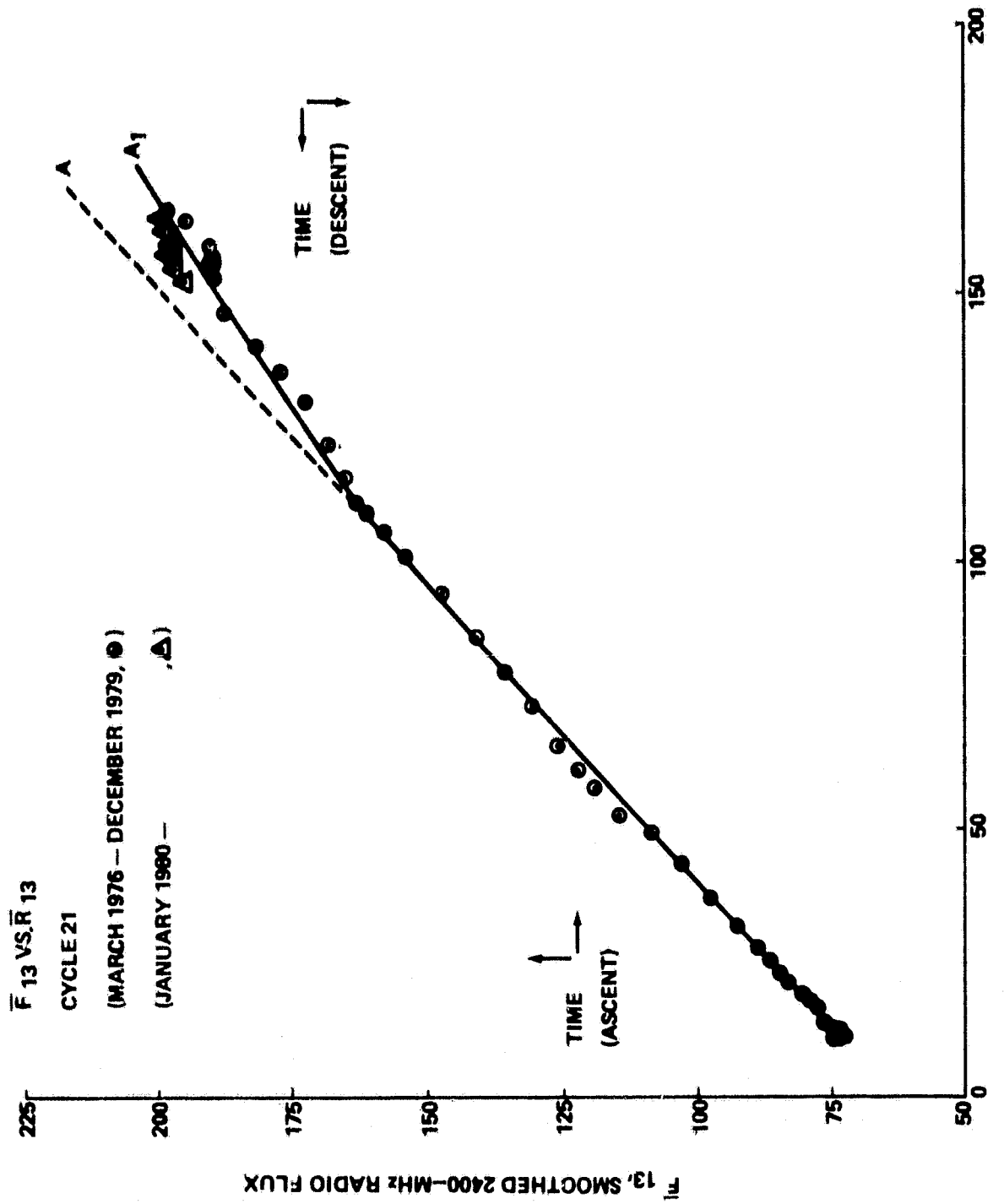

Figure 13. $\bar{F}_{13}$ versus $\bar{R}_{13}$ for ascending portion (⊙) and descending portion (△) cycle 21. Line equations given in text.

and

$$\text{Line } A_1 \text{ (for } 110 \leq \bar{R}_{13} \leq 166) \qquad \bar{F}_{13} = 0.65\,\bar{R}_{13} + 90 \qquad (12)$$

IV. LATE CYCLE 21: A LOOK AT THE SPACELAB 2 ERA

Rosendahl [12] has briefly described the Spacelab 2 instrument complement. Essentially, it is an astrophysics and solar physics mission with additional studies being conducted in life sciences, upper atmosphere, space plasma physics, and space technology. The solar instruments are mounted on a pointing system and view the Sun in a fashion similar to the Skylab-ATM (Apollo Telescope Mount), utilizing the services of a human being in the control and operational loop. Spacelab 2 had tentatively been planned for launch in April 1981, or about a year or so past solar maximum; however, much like Skylab, it will probably fly late in the solar cycle (presently, it is tentatively set for launch in November 1984), just prior to the minimum of the subsequent cycle. Consequently, the behavior of the Sun during the Spacelab 2 timeframe may be quite similar to that of the Skylab mission period of 1973-74.

It was previously shown that cycle 20 $\bar{R}_{MAX}$ occurred in October 1968 with a value of 110.6. Also, cycle 21 $\bar{R}_{MIN}$ occurred in March 1976 with a value of 12.4. Thus, mathematically speaking, cycle 20 decayed at the rate of about 1.103 units per month. Variation about this smooth-line decay of about 20 percent was observed. Cycle 21 $\bar{R}_{MAX}$ occurred in December 1979 with a value of 166.3, and cycle 22 $\bar{R}_{MIN}$ is projected to occur approximately February 1987 (based on the MIN-MIN mean 8-21; Table 1) with a value of approximately 10.4 (based on Figure 3). Thus, cycle 21 is projected to decay at the rate of about 1.813 units per month. Since the launch of Spacelab 2 is tentatively set for late 1984, an approximate value for $\bar{R}_{13}$ is 59.3 ± 20 percent, or between 47.4 and 71.2 if its decline is similar to cycle 20. (The Skylab period $\bar{R}_{13}$ was about 35.) Using equation (11), $\bar{F}_{13}$ can be estimated to be about 115.8 ± 10 percent. Also, approximate levels of flare and eruptive activity can be projected, based on the equations in Section III. Thus, for the Spacelab 2 time frame, $\bar{N}_{13}$ (≥1) can be estimated to be about 27.3 [from equation (4)], $\bar{N}_{13}$ to be about 148.3 [from equation (8)], and $\bar{N}_{13}$ (GRF) to be about 28.8 [from equation (10)]. These mean activity numbers suggest that, in a statistical sense, about one major flare per day, about four subflares per day, and about one GRF-radio event per day during the Spacelab 2 flight can be expected. Thus, Spacelab 2, having a mission duration of approximately 1 week, may record as many as 35 flares (7 of which will be major flares) and 7 eruptives. (These numbers have not been reduced to account for orbital day/night or timeline constraints.)

In addition to flare and eruptive activity, a major scientific objective will be the study of the morphology and evolution of active regions (including ephemeral regions). So, it would be of interest to estimate the number of regions available for observation during Spacelab 2. Allen [9] has stated that at sunspot minimum the mean number of individual spots per R_z is 0.70, the mean number of sunspot groups per R_z is 0.097, and the mean number of individual spots per group is 7.3. Similarly, at sunspot maximum, he gives the mean number of individual spots per R_z as 0.87,

the mean number of sunspot groups per R_z as 0.083, and the mean number of individual spots per group as 11.0. Since the mean decay time from maximum to minimum is approximately 82 months and the Spacelab 2 tentatively scheduled launch is approximately 59 months after solar maximum, one could interpolate between the preceding mean numbers and generate approximate mean numbers for the parameters applicable to the Spacelab 2 mission period. Hence, the following approximate relationships can be deduced:

Mean number of individual spots per R_z ≈ 0.75

Mean number of sunspot groups per R_z ≈ 0.093

Mean number of individual spots per group ≈ 8.3 .

Since $\bar{R}_{13}$ has been calculated to be about 59.3 ± 20 percent during Spacelab 2, one can estimate the range of R_z to be about 59.3 ± 50 percent, or between 29.7 and 89. This implies that the mean number of individual spots on the Sun will be between 22.3 and 66.8 (mean 44.5) and the mean number of sunspot groups will be between 2.8 and 8.3 (mean 5.5). If cycle 21 behaves as did cycle 20, then during the decline of the cycle the Sun may have a very active hemisphere occurring about every 2 weeks and a very quiet hemisphere [13]; thus, mission planners will necessarily have to monitor solar activity levels prior to launch to ensure that Spacelab 2 mission objectives can be met. (It is important to re-emphasize that the analysis given in this section is for the statistically averaged Sun and must be viewed in that context.)

V. SUNSPOT CYCLE 22

Following the approach of Sections III and IV, Figures 1 through 3 and Table 1 could be used to predict the occurrence of solar minimum and maximum and their appropriate smoothed sunspot number values and to make some general remarks about cycle 22, the next sunspot cycle. Therefore, since cycle 21 $\bar{R}_{MIN}$ is known to have occurred in March 1976 with a value of 12.4 and $\bar{R}_{MAX}$ in December 1979 with a value of 166.3, the conclusions are reached that cycle 22 $\bar{R}_{MIN}$ will occur between October 1986 (based on Table 1, MAX-MIN time interval) and February 1987 (based on Table 1, MIN-MIN time interval) with a value of 10.4 (based on Figure 3) and that $\bar{R}_{MAX}$ will occur between November-December 1990 (based on Table 1, MAX-MAX time interval and MIN-MAX time interval, assuming an $\bar{R}_{MIN}$ occurrence of October 1976) and March 1991 (based on Table 1 MIN-MAX time interval, assuming an $\bar{R}_{MIN}$ occurrence of February 1987) with a value of approximately 150. Cycle 22 will end about September 1997 to January 1998, based on an application of Table 1 results to the minimum and maximum occurrence dates projected for cycle 22, as discussed previously. Thus, cycle 22 is projected to have a cycle duration of approximately 128 to 136 months. Also, since it is an even-numbered cycle, if it follows the pattern of previous solar cycles, the leading sunspots in the northern solar hemisphere will have a south-seeking pole uppermost on the Sun's surface; i.e., the magnetic field will be inwards through the Sun's surface in the northern hemisphere. (The Hale magnetic cycle is approximately 22 years.)

A second approach for determination of value $\bar{R}_{MAX}$ and $\bar{R}_{MIN}$, based on simple ratios, is given below. Using Figure 1 (or the tabular data given by Allen [9]), figures could be constructed based on the ratio of $\bar{R}_{MAX}$ to $\bar{R}_{MIN}$ for same cycle and subsequent cycle; i.e., (1) ratio the $\bar{R}_{MAX}$ and $\bar{R}_{MIN}$ values for the same cycle and plot the ratio versus solar cycle number and (2) ratio the $\bar{R}_{MAX}$ of a cycle and the $\bar{R}_{MIN}$ of the subsequent cycle and plot the ratio versus solar cycle number. Such has been done in Figures 14 and 15, respectively. The thin, single-humped curve, denoted $\bar{R}_{MAX}/\bar{R}_{MIN}$, peaking between cycles 15 and 16 in Figure 14 represents the ratio of the $\bar{R}_{MAX}$ and $\bar{R}_{MIN}$ cosine-related function, graphed in Figure 3, for the same-numbered solar cycle. For example, the dot (⊙) for cycle 9 is the ratio of the actual $\bar{R}_{MAX}$ to $\bar{R}_{MIN}$ values for cycle 9, and the line (in Fig. 14) just above that dot represents the ratio of the cosine-related equation for $\bar{R}_{MAX}$ and $\bar{R}_{MIN}$ (drawn in Fig. 3) which for cycle 9 is ≈168/11 or ≈15.3. The line appears to best fit odd-numbered cycles, although wide error bars are associated with it, particularly for cycle numbers 15 and 19. The even-numbered cycles appear to be best fit by the broad line having the form $\overline{R}_E = A_{MAX} \cos \theta + B_{MAX}$, where $A_{MAX} = 12.5$, $B_{MAX} = 22.5$ and the cosine function has a period of 176 years (which, coincidentally, is approximately twice the Gleissberg cycle [1]). $\overline{R}_E$ denotes the appropriate ratio of $\bar{R}_{MAX}$ to $\bar{R}_{MIN}$ (same cycle).

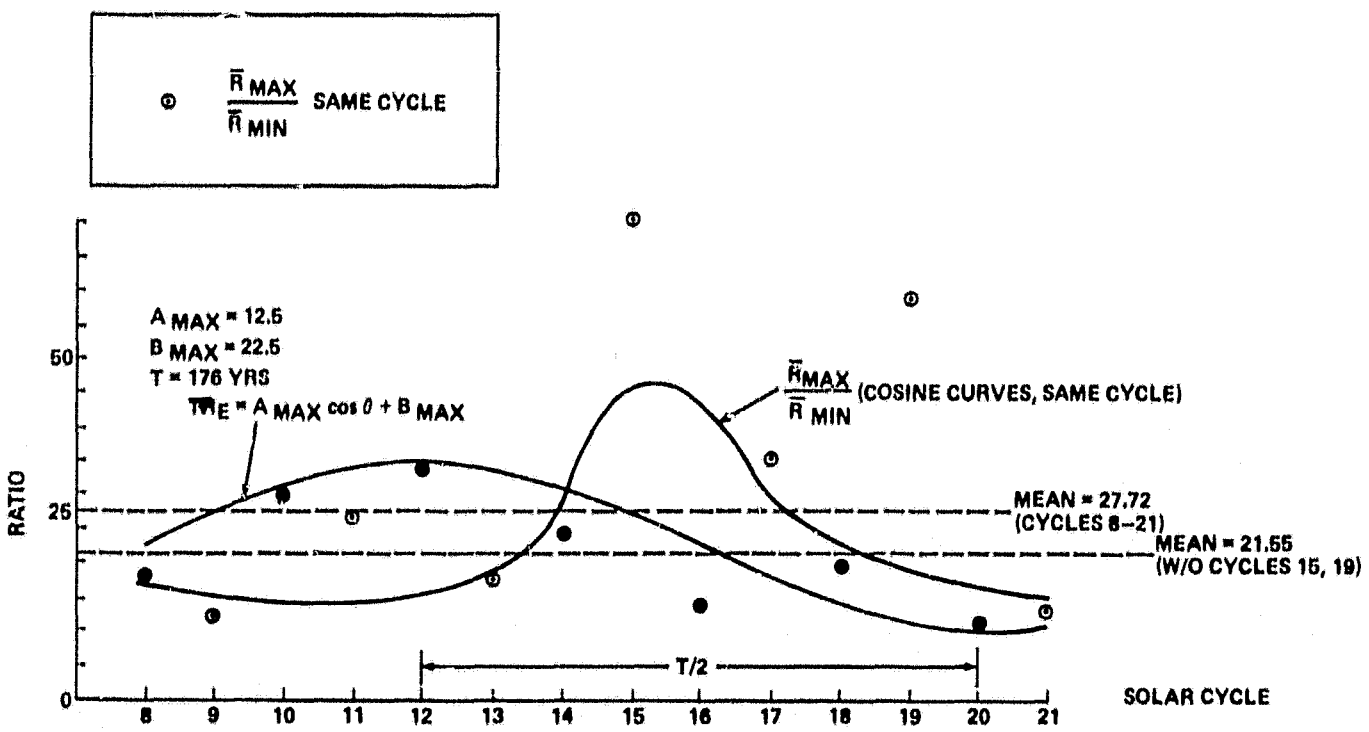

Figure 14. Variation of $\bar{R}_{MAX}/\bar{R}_{MIN}$ cycles 8 through 21, where $\bar{R}_{MAX}$ and $\bar{R}_{MIN}$ are for same cycle. Lines explained in text.

Figure 15 is similar to Figure 14 except it plots subsequent cycles; i.e., $\bar{R}_{MAX}$ present cycle to $\bar{R}_{MIN}$ subsequent cycle. Again, the thin, single-humped curve, denoted $\bar{R}_{MAX}/\bar{R}_{MIN}$, peaking at cycle 14 in Figure 15 represents the ratio of the $\bar{R}_{MAX}$ and $\bar{R}_{MIN}$ cosine-related functions, graphed in Figure 3, for subsequent solar cycles. For example, the triangle (▲) for cycle 10 is the ratio of the actual $\bar{R}_{MAX}$ value for cycle 10 to the actual $\bar{R}_{MIN}$ value for cycle 11, and the line (in Fig. 15) just below that triangle represents the ratio of the cosine-related equations for $\bar{R}_{MAX}$ and $\bar{R}_{MIN}$ (in Fig. 3) which for cycle 10-11 is ∿150/8.7 or ∿17.2. The line appears to best fit even-numbered cycles, although the actual cycle 18 value is somewhat higher than the ratio-derived value (line). The odd-numbered cycles appear to be best fit by the broad line having the form $TR_o = A_{MAX} \cos \theta + B_{MAX}$, where A_{MAX} = 20, B_{MAX} = 35, and the cosine function has a period of 132 years. TR_o denotes the appropriate ratio of $\bar{R}_{MAX}$ to $\bar{R}_{MIN}$ (subsequent cycle).

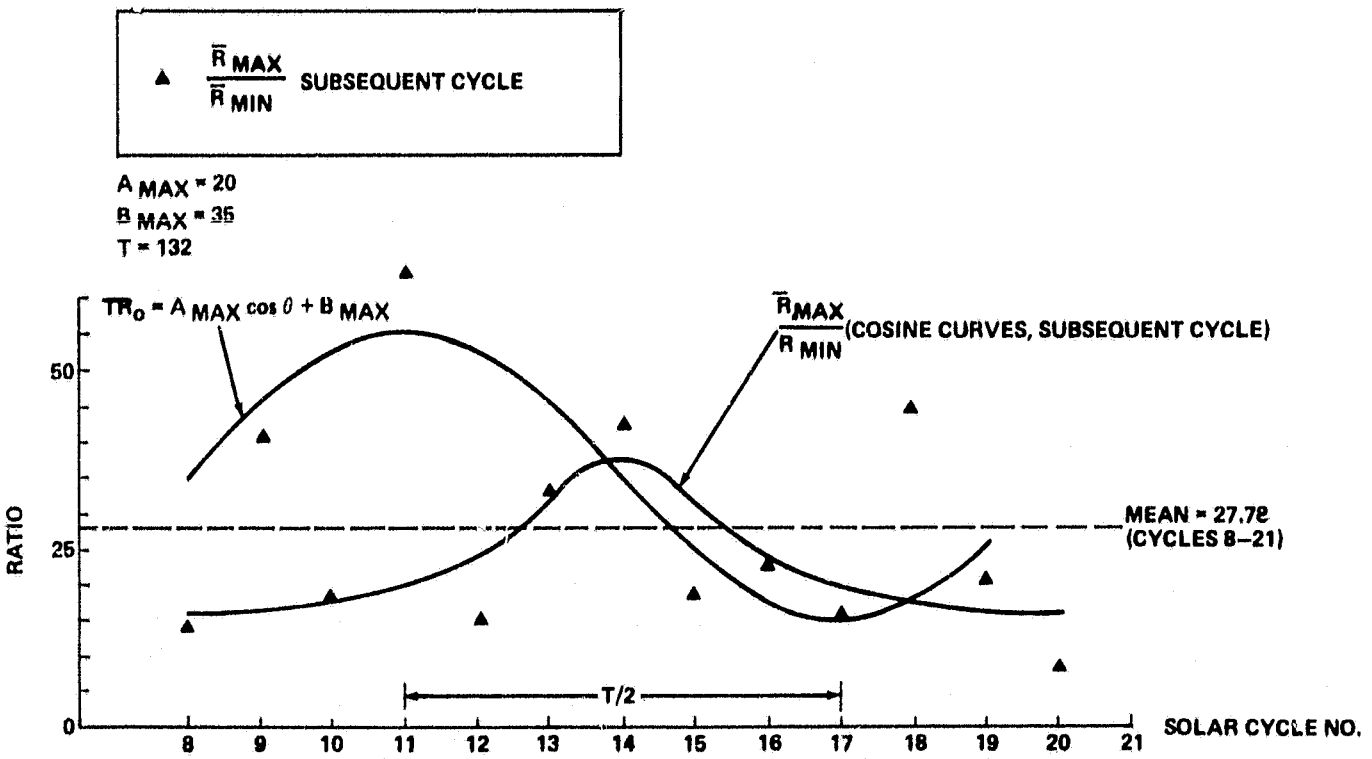

Figure 15. Variation of $\bar{R}_{MAX}/\bar{R}_{MIN}$ cycles 8 through 21, where $\bar{R}_{MIN}$ is for cycle subsequent to $\bar{R}_{MAX}$-determined cycle. Line equations explained in text.

Following the aforementioned approach (based on Figs. 14 and 15), cycle 22 is projected to have an $\bar{R}_{MAX}$ value between ∿145.6 and 148.7, based on the $\mathbf{R}_E$ and $\bar{R}_{MAX}/\bar{R}_{MIN}$ curves, respectively, for same cycle and given $\bar{R}_{MIN} = 10.4$. Cycle 22 is projected to have an $\bar{R}_{MIN}$ value between ∿4 and 10.4, based on the $\mathbf{R}_o$ and $\bar{R}_{MAX}/\bar{R}_{MIN}$ curves, respectively, for subsequent cycle and given $\bar{R}_{MAX}$ cycle 21 equal to 166.3. Using these $\bar{R}_{MIN}$ values for cycle 22, $\bar{R}_{MAX}$ for cycle 22 is also projected to be ∿56, based on $\bar{R}_{MIN} = 4$, or to be between ∿145.6 and 148.7, based on $\bar{R}_{MIN} = 10.4$, as above. Thus, the two described approaches suggest $\bar{R}_{MAX}$ to be approximately equal to 150, 148.7, 145.6, or 56, and $\bar{R}_{MIN}$ to be about 10.4, 10.4, or 4. Weighing each of the preceding $\bar{R}_{MAX}$ and $\bar{R}_{MIN}$ values equally and computing means suggest that, perhaps, the best-guess values for $\bar{R}_{MAX}$ and $\bar{R}_{MIN}$ for cycle 22 are approximately 125.1 and 8.3, respectively, or incorporating 30 percent error bars, $\bar{R}_{MAX}$ (cycle 22) = 125.1 ± 37.5 and $\bar{R}_{MIN}$ (cycle 22) = 8.3 ± 2.5.

If the behavior of cycle 22 follows that of cycle 21, then the approximate number of flares and GRF radio events and level of 2800 MHz radio emission can be estimated, based on the formulae of Section III, for sunspot minimum and maximum conditions. Hence, at $\bar{R}_{MIN}$ (cycle 22), the following would be anticipated: $\bar{N}_{13}$ (≥1) = 2.8 ± 0.8, $\bar{N}_{13}$ = 22 ± 6.6, $\bar{N}_{13}$ (GRF) = 10.5 ± 3.2, and $\bar{F}_{13}$ = 70.4 ± 21.1; and for $\bar{R}_{MAX}$ (cycle 22): $\bar{N}_{13}$ (≥1) = 42.5 ± 12.8, $\bar{N}_{13}$ = 353.8 ± 106.1, $\bar{N}_{13}$ (GRF) = 59.6 ± 17.9, and $\bar{F}_{13}$ = 174.3 ± 52.3. $\bar{F}_{13}$ at $\bar{R}_{MIN}$ and $\bar{R}_{MAX}$ can also be estimated from comments regarding Figure 5; i.e., at $\bar{R}_{MIN}$, $\bar{F}_{13}/\bar{R}_{13}$ is about 6 (for cycle 21), implying $\bar{F}_{13}$ (cycle 22) equal to ∿49.8, and $\bar{F}_{13}/\bar{R}_{13}$ is about 1.2 at $\bar{R}_{MAX}$ (based on cycle 20 and 21), suggesting $\bar{F}_{13}$ (cycle 22) equal to ∿150.1. Caution must be urged in using these numbers, since the assumption that cycle 22 behaves essentially as cycle 21 may not be valid. [It is of interest to note, however, that the Skylab period had an $\bar{R}_{13}$ value of ∿35, which implies a value of $\bar{F}_{13}$ to be ∿94.2 [based on equation (11)], $\bar{N}_{13}$ (≥1) ∿ 11.9 to 16.1 [based on equations (3) and (4), respectively], $\bar{N}_{13}$ ∿ 87.5 to 97.6 [based on equations (7) and (8), respectively], and $\bar{N}_{13}$ (GRF) ∿ 20.1 to 33.4 [based on equations (9) and (10), respectively]. Actual values for $\bar{F}_{13}$ and $\bar{N}_{13}$ (≥1) were ∿86 and ∿19. Thus, $\bar{F}_{13}$ was actually slightly less than would have been predicted and $\bar{N}_{13}$ (≥1) slightly more. Actual number counts for $\bar{N}_{13}$ and $\bar{N}_{13}$ (GRF) have not been made, so comparison cannot be accomplished.]

VI. CONCLUSIONS

Sunspot variation is a phenomenon that has been apparent on the Sun for at least hundreds of years (if not longer). This report briefly discussed the solar cycle sunspot variation, particularly for cycle numbers 8 through 21. It was shown that the variation of sunpot maxima and minima values could be simply described, in an approximate way, by arbitrarily chosen cosine-related periodic functions (with a period of 132 years). Using this simplified approach and based on $\bar{R}_{MAX}$ and $\bar{R}_{MIN}$ occurrence dates for cycle 20, it was determined that a projection of cycle 21 was

observed to agree quite closely with actual values. Formulae were given relating numbers of flares, major flares, and GRF-radio events to $\bar{R}_{13}$, as well as $\bar{F}_{13}$ to $\bar{R}_{13}$. Based on the decline of cycle 20 and, predominately, on the rise portion of cycle 21, a prediction of activity levels was made for the Spacelab 2 mission time frame (late 1984). Finally, a prediction of activity levels was made for cycle 22. Tables 2, 3, and 4 summarize the findings for cycle 21, the Spacelab 2 mission time frame, and cycle 22, respectively.

With the advent of the Shuttle [actually the Space Transportation System (STS)], solar physics may be entering a new era of unprecedented opportunity to study the multifarious solar cycle dependent relationships and other phenomena. These future missions (e.g., Spacelab 2 and others, such as SCADM Solar Cycle and Dynamics Mission [14]) will have mission and scientific objectives which often may be solar cycle dependent.[3] This report is intended to serve as an aid to planners of these missions.

TABLE 2. SUMMARY OF CYCLE 21

Parameter	Value	Remarks
Date Sunspot Minimum	March 1976	1
Date Sunspot Maximum	December 1979	1
Cycle Duration (months)	127-132	2,3
Ascent Duration (months)	45	1
Descent Duration (months)	82-87	2,3
$\bar{R}_{MIN}$	12.4	1
$\bar{R}_{MAX}$	166.3	1,4
$\bar{F}_{MIN}$	73.3	1
$\bar{F}_{MAX}$	198.0	1,4
$\bar{N}_{MIN}$	27.8	1
$\bar{N}_{MAX}$	438.0	1,4
$\bar{N}_{MIN}$ (-1)	2.7	1
$\bar{N}_{MAX}$ (-1)	71.5	1,4
$\bar{N}_{MIN}$ (GRF)	10.7	1
$\bar{N}_{MAX}$ (GRF)	66.5	1,4

Remarks: 1 - Observed.
2 - Predicted.
3 - Assumes Cycle 22 begins October 1986-February 1987, based on application of Table 1 mean time intervals. (MIN-MIN and MAX-MIN.)
4 - Assumes maximum occurred prior to August 1980.

3. Schatten and Sofia [15] have recently investigated the Schwarzchild criterion for convection in the presence of a magnetic field and believe that their results may be of importance for solar variability.

TABLE 3. SUMMARY OF SPACELAB 2 MISSION TIME-FRAME PROJECTIONS

Parameter	Value	Remarks
Cycle 21 Sunspot Maximum	December 1979	1
Cycle 22 Sunspot Minimum	February 1987	2,3
Cycle 21 Duration (months)	132	2,3
Cycle 21 Descent Duration (months)	87	2,3
Cycle 21 $\bar{R}_{MAX}$	166.3	1,4
Cycle 22 $\bar{R}_{MIN}$	10.4	2,5
Cycle 21 $\bar{R}_{13}$ Decay Rate (units/month)	1.813	2,3
$\bar{R}_{13}$ (November 1984)	59.3	2,6
$\bar{F}_{13}$ (November 1984)	115.8	2,7
$\bar{N}_{13}$ (November 1984)	148.3	2,8
$\hat{N}_{13}$ (-1) (November 1984)	27.3	2,9
$\bar{N}_{13}$ (GRF) (November 1984)	28.8	2,10
Number Observable Flares During Mission	~35	2,11
Number Observable Major Flares During Mission	~7	2,11
Number Observable Eruptives	~7	2,11

Remarks:
1 - Observed.
2 - Predicted.
3 - Based on Table 1 (MIN-MIN).
4 - Assumes maximum occurred prior to August 1980.
5 - Based on Figure 3.
6 - Assumes $\bar{R}_{MAX}$ occurrence is correctly known and $\bar{R}_{13}$ decay rate is accurate.
7 - Based on equation (11).
8 - Based on equation (8).
9 - Based on equation (4).
10 - Based on equation (10).
11 - Based on 1-week mission duration; no correction (reduction) has been made for orbital day/night or timeline constraints.

TABLE 4. PROJECTION FOR CYCLE 22

Parameter	Value	Remarks
Date Sunspot Minimum	October 1986-February 1987	1
Date Sunspot Maximum	November 1990-March 1991	1
Cycle Duration (months)	128-136	2
Ascent Duration (months)	45-53	2
Descent Duration (months)	75-91	2
$\bar{R}_{MIN}$	8.3 ± 2.5	3
R_{MAX}	125 ± 37.5	3
$\bar{F}_{MIN}$	70.4 ± 21.1	4
$\bar{F}_{MAX}$	174.3 ± 52.3	4
$\bar{N}_{MIN}$	22 ± 6.6	4
$\bar{N}_{MAX}$	353.8 ± 106.1	4
$\bar{N}_{MIN}$ (-1)	2.8 ± 0.8	4
$\bar{N}_{MAX}$ (-1)	42.5 ± 12.8	4
$\bar{N}_{MIN}$ (GRF)	10.5 ± 3.2	4
$\bar{N}_{MAX}$ (GRF)	59.6 ± 17.9	

Remarks: 1 - Based on Tables 1 and 2.
2 - Straight-forward calculation.
3 - Mean based on numbers derived from Figures 3, 14, and 15, and assuming 30 percent error bars; actual values suggested for $\bar{R}_{MAX}$ include 150, 148.7, 145.6, and 56; actual values suggested for $\bar{R}_{MIN}$ include 10.4 and 4; see text.
4 - Based on equations given in text; assumes cycle 22 behaves similarly to cycle 21.

Figures A-1 through A-5 are scatter diagrams comparing raw monthly mean values with their smoothed monthly mean values. Figure A-1 is the scatter diagram comparing R_z and $\bar{R}_{13}$. Figure A-2 compares F_{2800} and $\bar{F}_{13}$, Figure A-3 N(≥1) and $\bar{N}_{13}$ (≥1), Figure A-4 N and $\bar{N}_{13}$, and Figure A-5 N(GRF) and $\bar{N}_{13}$ (GRF). The dark line running diagonally from lower-left to upper-right on each of the figures is the 1-to-1 correlation line. The dashed lines running diagonally from lower-left to upper-right on each figure represent the ±20 percent and ±30 percent departure spreads. It is observed that sunspot numbers vary by about 20 percent at high sunspot numbers and by 30 percent or more near solar minimum. The 2800-MHz radio emission, conversely, varies by only a few percent at sunspot minimum and by 20 percent or less at high sunspot number. Major flare variation is much broader, being 30 percent or more, while the general class of flares and GRF events show variation of usually less than 20 percent near sunspot maximum and 30 percent or more near sunspot minimum.

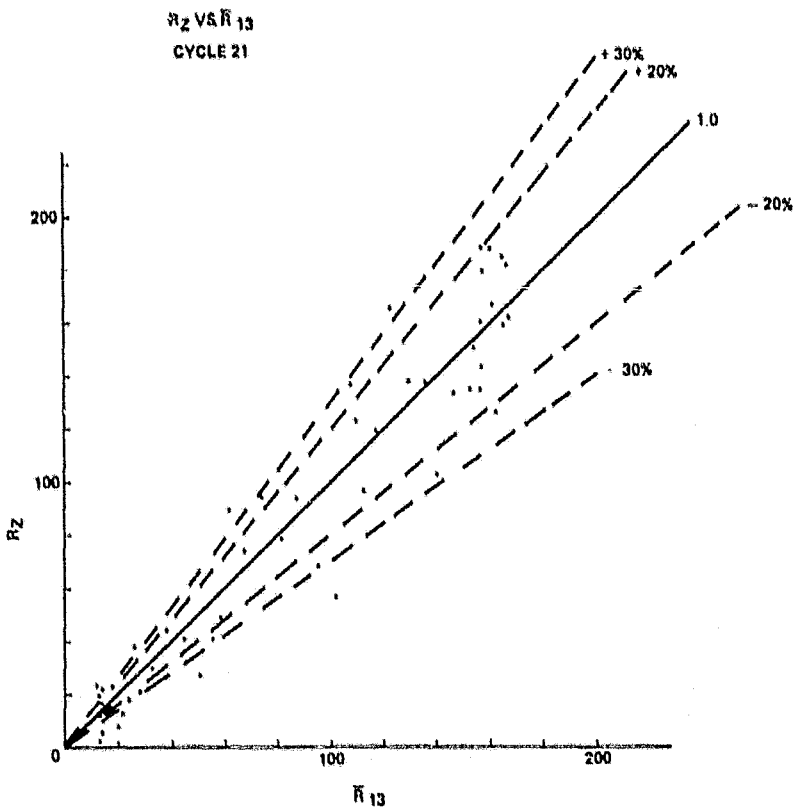

Figure A-1. R_z versus $\bar{R}_{13}$ cycle 21 scatter plot.

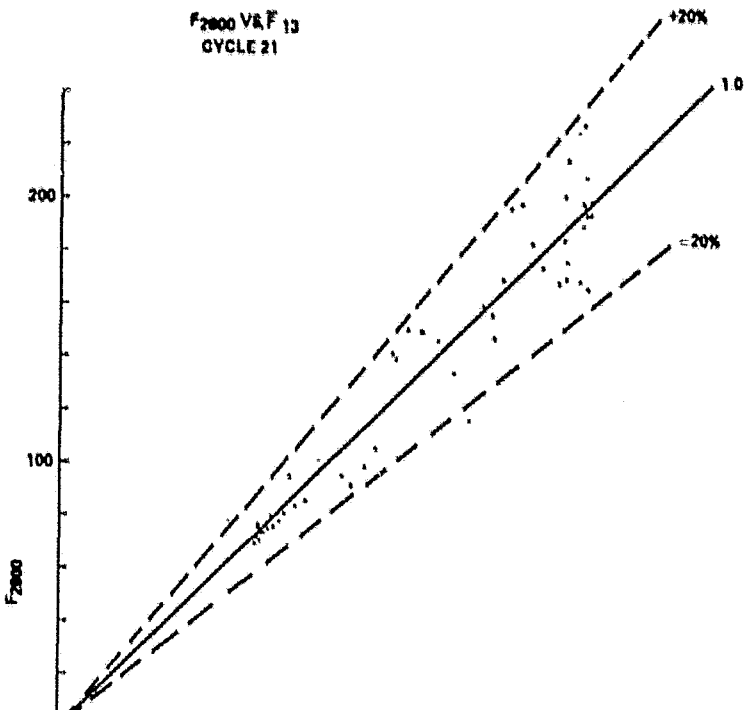

Figure A-2. F_{2800} versus $\bar{F}_{13}$ cycle 21 scatter plot.

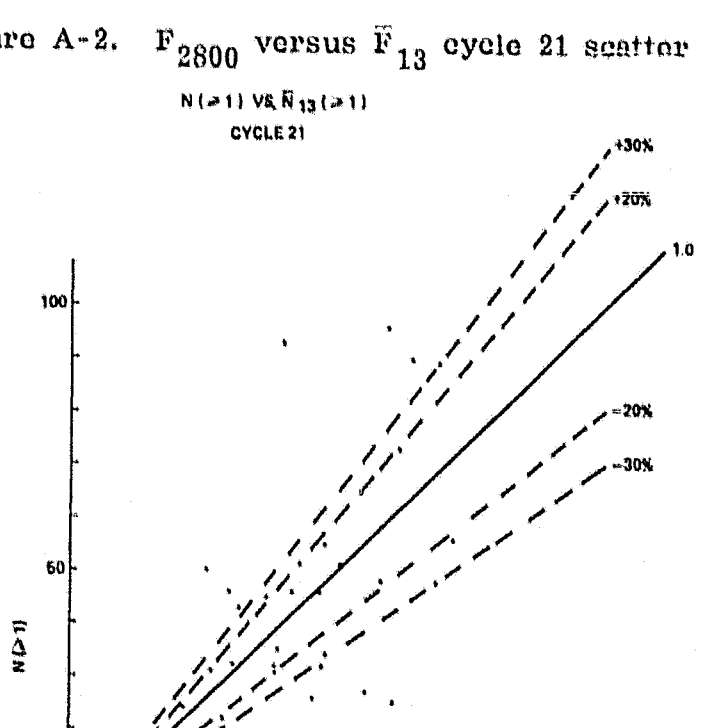

Figure A-3. N(≥1) versus $\bar{N}_{13}$ (≥1) cycle 21 scatter plot.

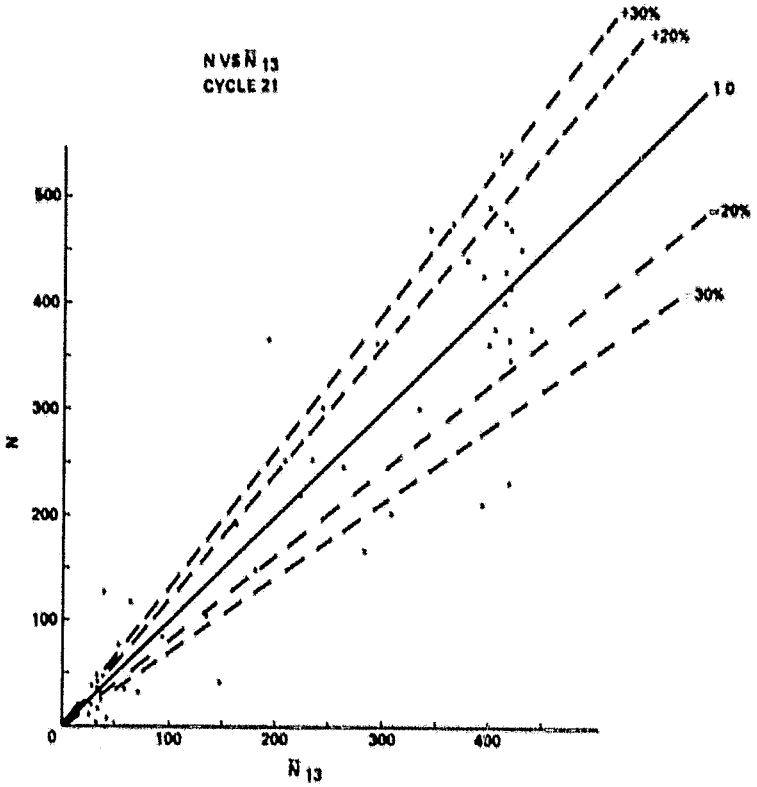

Figure A-4. N versus $\bar{N}_{13}$ cycle 21 scatter plot.

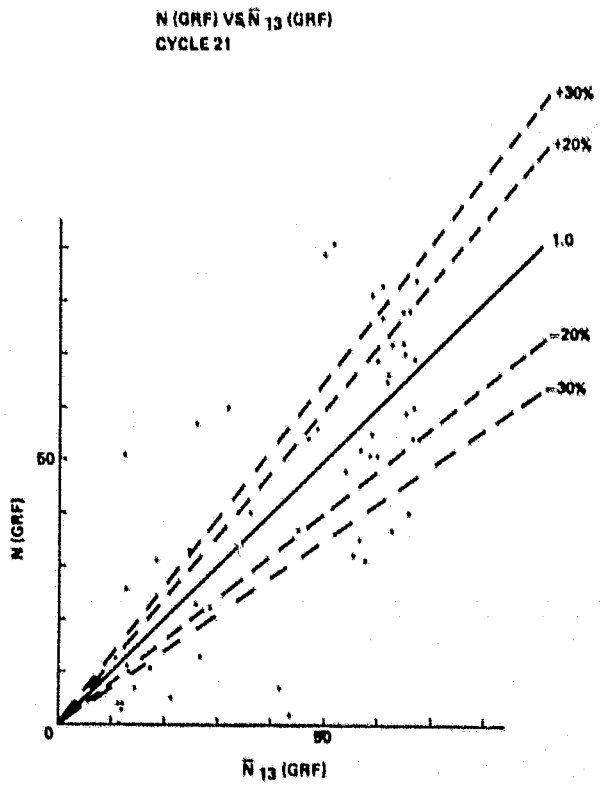

Figure A-5. N(GRF) versus $\bar{N}_{13}$ (GRF) cycle 21 scatter plot.

REFERENCES

1. Herman, J. R. and Goldberg, R. A.: Sun, Weather, and Climate. NASA SP-426, NASA Washington, D.C., 1978, pp. 12-21.

2. Eddy, J. A.: Historical Evidence for the Existence of the Solar Cycle. The Solar Output and Its Variation, edited by O. R. White, Colorado Associated University Press, Boulder, CO, 1977, pp. 51-71.

3. Howard, R.: 2. Solar Cycle, Solar Rotation and Large-Scale Circulation. Illustrated Glossary for Solar-Terrestrial Physics, edited by A. Bruzek and C. J. Durrant, Astrophysics and Space Science Library, vol. 69, D. Reidel Publ. Co., Dordrecht, Holland, 1977, pp. 7-12.

4. Howard, R.: Global Velocity Fields of the Sun and the Activity Cycle. American Scientist, vol. 69, January-February, 1981, pp. 29-36.

5. Sheeley, N. R., Jr., Bohlin, J. D., Brueckner, G. E., Purcell, J. D., Scherrer, V. E., Tousey, R., Smith, J. B., Jr., Speich, D. M., Tandberg-Hanssen, E., Wilson, R. M., deLoach, A. C., Hoover, R. B., and McGuire, J. P.: Coronal Changes Associated with a Disappearing Filament. Solar Phys., vol. 45, 1975, pp. 377-392.

6. Webb, D. F., Krieger, A. S., and Rust, D. M.: Coronal X-Ray Enhancements Associated with $H\alpha$ Filament Disappearances. Solar Phys., vol. 48, 1976, pp. 159-186.

7. Smith, J. B., Jr., Speich, D. M., Wilson, R. M., and Reichmann, E. J.: Long Duration Soft X-Ray Transients: Physical Parameters and Morphology. Contributed Papers to the Study of Travelling Interplanetary Phenomena/1977, edited by M. A. Shea, D. R. Smart, and S. T. Wu, AFGL-TR-77-0309 (Special Report No. 209), Air Force Geophysics Laboratory, Hanscom AFB, MA, December 29, 1977, pp. 3-21.

8. Fisher, R., Garcia, C. J., and Seagraves, P.: On the Coronal Transient-Eruptive Prominence of 1980 August 5. Astrophys. J., vol. 246, 1981, pp. L161-L164.

9. Allen, C. W.: Astrophysical Quantities (Third Edition). University of London, The Athlone Press, London, England, 1973, pp. 181-184.

10. Wilson, R. M.: Skylab ATM/S-056 X-Ray Event Analyzer Observations Versus Solar Flare Activity: An Event Compilation. NASA TM X-73363, Marshall Space Flight Center, AL, January 1977.

11. Dodson-Prince, H. W. and Bruzek, A.: 9. Flares and Associated Phenomena. Illustrated Glossary for Solar-Terrestrial Physics. Edited by A. Bruzek and C. J. Durrant, Astrophysics and Space Science Library, vol. 69, D. Reidel Publ. Co., Dordrecht, Holland, 1977, pp. 81-96.

12. Rosendahl, J. D.: The Spacelab 2 Mission. Sky and Telescope, vol. 56, June 1978, pp. 462-464.

13. Speich, D. M., Smith, J. B., Jr., Wilson, R. M., and McIntosh, P. S.: Solar Activity During Skylab – Its Distribution and Relation to Coronal Holes. NASA TM-78166, Marshall Space Flight Center, AL, April 1978.

14. Study of the Solar Cycle from Space. NASA Conference Publication 2098, Goddard Space Flight Center, Greenbelt, MD, February 1980.

15. Schatten, K. H., and Sofia, S.: The Schwarzschild Criterion for Convection in the Presence of a Magnetic Field. Astrophys. Letters, vol. 21, 1981, pp. 93-96.

APPROVAL

SUNSPOT VARIATION AND SELECTED ASSOCIATED PHENOMENA: A LOOK AT SOLAR CYCLE 21 AND BEYOND

By Robert M. Wilson

The information in this report has been reviewed for technical content. Review of any information concerning Department of Defense or nuclear energy activities or programs has been made by the MSFC Security Classification Officer. This report, in its entirety, has been determined to be unclassified.

Ernest Hildner

ERNEST HILDNER
Chief, Solar Sciences Branch

Charles Richard Chappell

CHARLES R. CHAPPELL
Chief, Solar-Terrestrial Physics Division

C. R. O'DELL
Acting Director, Space Sciences Laboratory

☆U.S. GOVERNMENT PRINTING OFFICE: 1982-546-071/201